Journal of Medicinal Chemistry

pubs.acs.org/jmc

Article

Structural Determinants for the Mode of Action of Imidazopyridine DS2 at δ-Containing γ-Aminobutyric Acid Type A Receptors

Frederik Rostrup, Christina B. Falk-Petersen, Kasper Harpsøe, Stine Buchleithner, Irene Conforti, Sascha Jung, David E. Gloriam, Tanja Schirmeister, Petrine Wellendorph, and Bente Frølund*

Cite This: J. Med. Chem. 2021, 64, 4730−4743

Read Online

ACCESS | Metrics & More | Article Recommendations | Supporting Information

ABSTRACT: Despite the therapeutic relevance of δ-containing γ-aminobutyric acid type A receptors ($GABA_A$Rs) and the need for δ-selective compounds, the structural determinants for the mode and molecular site of action of δ-selective positive allosteric modulator imidazo[1,2-a]pyridine DS2 remain elusive. To guide the quest for insight, we synthesized a series of DS2 analogues guided by a structural receptor model. Using a fluorescence-based fluorometric imaging plate reader membrane potential assay, we found that the δ-selectivity and the pharmacological profile are severely affected by substituents in the 5-position of the imidazopyridine core scaffold. Interestingly, the 5-methyl, 5-bromo, and 5-chloro DS2 analogues, **30**, **35**, and **36**, were shown to be superior to DS2 at α4β1δ as mid-high nanomolar potency δ-selective allosteric modulators, displaying 6−16 times higher potency than DS2. Of these, **30** also displayed at least 60-fold selectivity for α4β1δ over α4β1γ2 receptor subtypes representing a potential tool for the selective characterization of δ-containing $GABA_A$Rs in general.

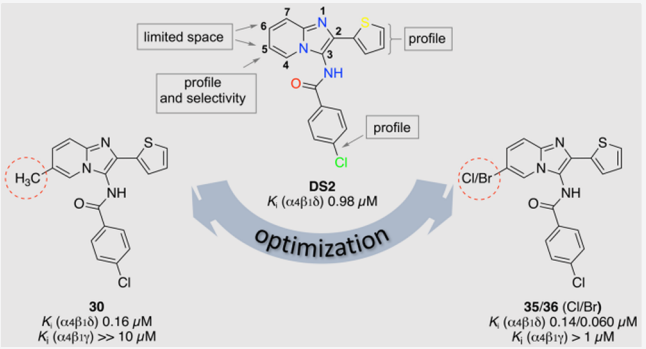

INTRODUCTION

γ-Aminobutyric acid (GABA) is a major inhibitory neurotransmitter in the central nervous system,[1] and it mediates its effect via the ionotropic γ-aminobutyric acid type A receptors ($GABA_A$Rs) and the metabotropic γ-aminobutyric acid type B receptors.[2] $GABA_A$Rs are clinically employed targets for numerous drugs, including anesthetics,[3] barbiturates,[4] and benzodiazepines[5] because of their sedative, anxiolytic, and anticonvulsant effects. $GABA_A$Rs form transmembrane heteropentameric complexes from at least 19 different subunits: α1−6, β1−3, γ1−3, ρ1−3, δ, θ, π, and ε.[6] The combination of subunits affects the subcellular localization and type of inhibition being mediated. The majority of $GABA_A$Rs have the general stoichiometry of 2α, 2β, and 1γ subunits and are typically located synaptically mediating fast and transient inhibition.[7] The synaptic $GABA_A$Rs are sensitive to high concentrations of GABA and are prone to desensitization. Extrasynaptic $GABA_A$Rs typically incorporate a δ-subunit. Although it is generally accepted that the δ-subunit in its cognate receptors simply replaces the γ-subunit with respect to arrangement,[28] this is still not unequivocally established.[26,29] Pharmacologically, extrasynaptic receptors are sensitive to low concentrations of GABA and mediate tonic inhibition, distinct from the fast and transient synaptic inhibition, and are less prone to desensitization.[8] As the δ-subunit-containing $GABA_A$Rs have been proposed to be implicated in, for example, alcoholism,[9] epilepsy,[8] and major depression disorder,[10] these receptors have been in focus in the last few decades as potential drug targets (for reviews, see, e.g., refs 11. and 12). To date, few compounds exhibit δ-selectivity[13,14] including imidazo[1,2-a]pyridine DS2 (Figure 1), shown by Jensen et al. to be a functionally selective α4/6β3δ positive allosteric modulator (PAM), relative to its action at α4β3γ2 and α1β3γ2 receptors.[15] In addition, DS2 has been shown to selectively modulate α4β1/3δ over α4β1/3 receptors in 1−10 μM concentrations. Although DS2 does not appear to pass the blood−brain barrier in rats and mice,[15] we recently reported uptake of a ^{11}C-labeled DS2 analogue, [^{11}C]DS2OMe (Figure 1) into the pig brain.[16]

A previous structure−activity relationship (SAR) study on the direct agonist effect of DS2 and the 6,8-dibromo analogue, DS1 (Figure 1), reported that DS1, but not DS2, is able to increase [^{3}H]-ethynylbicyclooethobenzoate ([^{3}H]-EBOB) binding to δ-containing $GABA_A$Rs in the absence of GABA.[17] EBOB is a potent noncompetitive $GABA_A$R

Received: December 15, 2020
Published: April 13, 2021

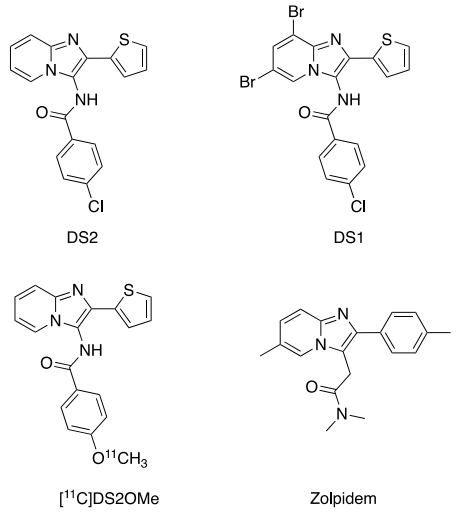

Figure 1. Chemical structures of the δ-selective $GABA_AR$ allosteric modulator, DS2, the positron emission tomography (PET) ligand candidate, [^{11}C]DS2OMe, the $GABA_AR$ allosteric agonist, DS1, and the standard benzodiazepine binding site ligand zolpidem.

antagonist that binds to the picrotoxinin binding site within the $GABA_AR$ ion channel.[18] [^{3}H]-EBOB binding is sensitive to conformational changes in the chloride-conducting channel, which can be mediated by increasing concentrations of GABA and/or affected by modulators in the presence or absence of GABA.[19−21] In the referred SAR study, two DS1 analogues were identified as δ-selective allosteric agonists in the absence of GABA.[17] However, both compounds lost their δ-selectivity in the presence of GABA, thus limiting their use for *in vivo* studies.[17]

Despite DS2 being an important tool compound[14,22,23] and regardless of extensive investigations, its molecular site of action remains elusive.[3,15] Herein, we describe our efforts to investigate the molecular determinants for the pharmacology of DS2 at $\alpha4\beta1\delta$ $GABA_ARs$ by probing the δ-selective modulatory effect on the activity of GABA using a fluorometric imaging plate reader (FLIPR) membrane potential (FMP) functional assay. Ultimately, we sought to assist future modeling and site-directed mutagenesis studies that could lead to the revelation of the undiscovered DS2 binding site.[15,17] Consequently, we expand the pharmacophore for the δ-selective allosteric effect on GABA modulation by introducing various synthesis strategies to structurally diversify the imidazopyridine scaffold of DS2 including a structural receptor model.

RESULTS AND DISCUSSION

Ligand Design. Based on the structural similarity between DS2 and the standard benzodiazepine binding site ligand zolpidem (Figure 1), we hypothesized that DS2 may bind in a benzodiazepine-like binding pocket at the intersubunit $\alpha4/\delta$-interface at $\alpha4\beta1\delta$ $GABA_ARs$. This extracellular domain (ECD) pocket has been referred to as the C-loop pocket,[24] and the existence of such a pocket at δ-containing $GABA_ARs$ has previously been debated.[15,25] The binding hypothesis is further challenged by the subunit stoichiometry and assembly of δ-$GABA_ARs$, which continues to be poorly understood.[26−29]

To rationally guide ligand design, we constructed a homology model of the ECD C-loop pocket at the $\alpha4/\delta$-interface using the cryogenic electron microscopy (cryoEM)

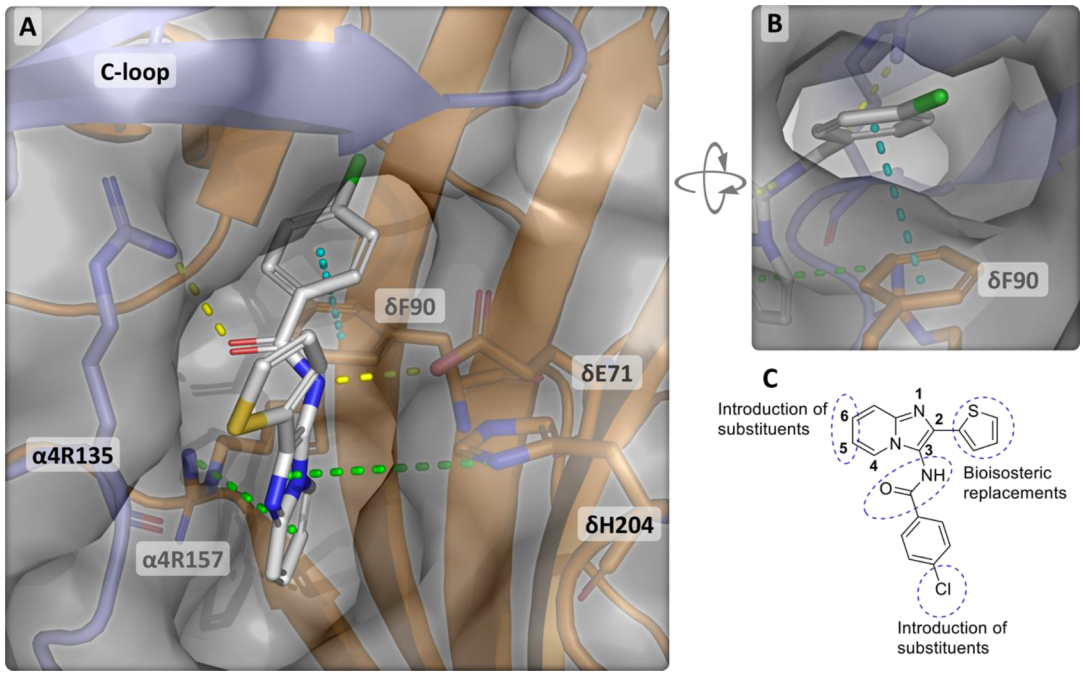

Figure 2. (A and B) Putative binding model of DS2 (white carbon atoms) in the extracellular part of the $GABA_AR$ interface between the $\alpha4$ (purple carbon atoms) and δ (orange carbon atoms) subunits showing charge-assisted hydrogen bonds and π-cation and π-π interactions between DS2 and the receptor (yellow, green, and cyan dotted lines, respectively), highlighted in another view in (B). The amino acid backbone of $GABA_ARs$ is depicted as a cartoon and selected residues as sticks, while the van der Waals surface is shown in transparent gray. In addition to the carbon atoms, which are colored according to molecules, oxygen, nitrogen, sulfur, and chlorine are red, blue, yellow, and green, respectively. (C) Schematic overview of the explored sites in the DS2 scaffold and numbering of the positions.

https://doi.org/10.1021/acs.jmedchem.0c02163
J. Med. Chem. 2021, 64, 4730−4743

structure of the human $\alpha1\beta2\gamma2$ $GABA_AR$ in complex with flumazenil (PDB-code: 6D6T)[30] as a template for our model. This was the first structure showing a binding in the benzodiazepine site, and though later published structures seem more relevant as templates, that is, containing positive modulators, diazepam, and alprazolam,[24] structural comparison shows very little variation in the binding site (Figure S1). The model was subsequently used for induced fit and extra precision (XP)-Glide docking of previously reported compounds.[17] The putative binding mode obtained for DS2 (Figure 2A,B) predicts the following specific interactions: (i) charge-assisted hydrogen bonds from the central amide to α4R135 and δE71, (ii) π-cation interaction from the imidazo[1,2-a]pyridine to δR157 and δH204, and (iii) π-stacking between the chlorophenyl and δF90. Additionally, other surrounding amino acids delineate the binding site, which are considered as a van der Waals surface, some in direct contact and some further away allowing space for substituents. As expected, there is a positional overlap of DS2 and diazepam (plus the very similar alprazolam) in the $\alpha4/\delta$- and $\alpha1/\gamma2$-interfaces with similar dimer interfaces and C-loop closure, but distinct interactions reflecting different modulators and binding sites (Figure S2).

To test the predicted binding mode, we systematically varied the structural scaffold of DS2, as depicted in Figure 2C. If our predicted binding mode is true, the amide functionality in position 3 (Figure 2C) with both a hydrogen bond donor and acceptor function should be crucial to modulation, which can be probed by bioisosteric replacement, exemplified by compounds **40** and **42** (Scheme 4). To this end, we examined the lack of aromatic interactions to the thiophene in position 2 (Figure 2C) and the available space from almost protruding out of the binding site by increasing the aromatic ring size and removing the aromaticity by compounds **18** and **22** (Schemes 1 and 2). Likewise, the chlorophenyl of DS2 is predicted to point into an unexplored area under the C-loop and even out

Scheme 1. Imidazo[1,2-a]Pyridine-3-Amine Synthesis Via the Groebke–Blackburn–Bienayme (GBB)-Multicomponent Reaction[a]

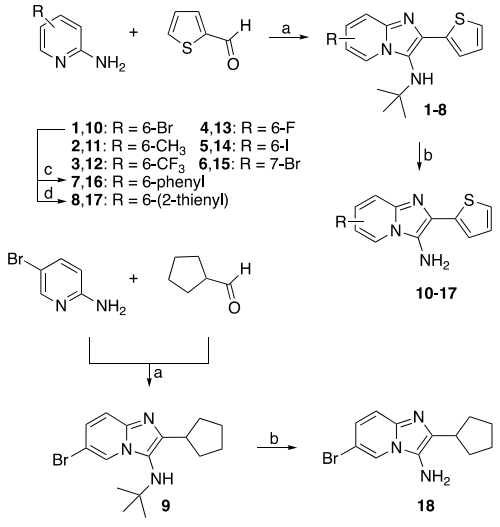

[a]Reagents and conditions: (a) *tert*-butyl isocyanide, NH_4Cl, toluene, and reflux; (b) 5 M HBr and 110 °C. (c) $Pd(PPh_3)_4$, Na_2CO_3, $PhB(OH)_2$, DME/H_2O, and reflux. (d) $Pd(PPh_3)_4$, Na_2CO_3, 2-thienylB$(OH)_2$, DME/H_2O, and reflux.

Scheme 2. Synthesis of 2-Substituted Imidazo[1,2-a]Pyridine-3-amine[a]

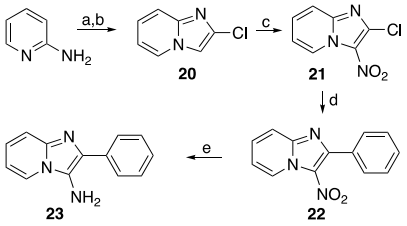

[a]Reagents and conditions: (a) 2-chloroacetic acid, Et_3N/H_2O, 90 °C to give 2-(2-iminopyridin-1(2*H*)-yl)acetic acid (**19**); (b) $POCl_3$, toluene, and reflux; (c) Conc. H_2SO_4, HNO_3, and 5 °C to rt.; (d) $Pd(PPh_3)_4$, DME/H_2O, Na_2CO_3, and reflux; (e) $SnCl_2$, MeOH, and reflux.

from the binding site leaving space for substituents (Figure 2B), which was challenged by compound **25** (Scheme 3). In contrast, the binding mode model shows limited to a fair amount of room for substitution possibilities in the 6- and 5-positions of the imidazo[1,2-a]pyridine, which was explored by compounds **27**, **28**, and **30–36** (Scheme 3).

Synthesis of Target Compounds. The new DS2 analogues **24–34** and **40** were synthesized as depicted in Schemes 1–4. Compound **35** and **36** were synthesized according to procedures reported in the literature.[17]

The 2-substituted imidazo-[1,2-a]pyridin-3-amides (**24–34**) were all obtained in a two-step procedure via the corresponding amines (**10–18**). Initially, one-step GBB-multicomponent reactions[31–33] with potassium cyanide, the respective 2-aminopyridines, aldehydes, and different Lewis acids were attempted to obtain **10**. However, byproduct formation, including formation of bicondensated adducts,[34] and poor starting material conversion resulted in low yields and unsuccessful workups. Alternatively, the *tert*-butyl-protected intermediates, imidazo-[1,2-a]pyridine-3-amines (**1–9**), were obtained in medium to high yield through similar GBB-multicomponent reactions[31–33] using the appropriate

Scheme 3. Synthesis of N-(2-Substituted Imidazo[1,2-a]Pyridin-3-yl)amides[a]

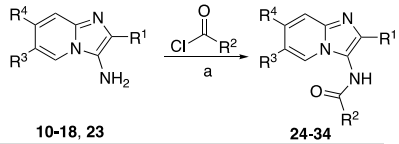

cmp	R^1	R^2	R^3	R^4
24	2-thienyl	Ph	Br	H
25	2-thienyl	4-PhO-Ph	Br	H
26	cyclopentyl	Ph	Br	H
27	2-thienyl	Ph	Ph	H
28	2-thienyl	Ph	2-thienyl	H
29	Ph	Ph	H	H
30	2-thienyl	4-Cl-Ph	CH_3	H
31	2-thienyl	4-Cl-Ph	CF_3	H
32	2-thienyl	4-Cl-Ph	F	H
33	2-thienyl	4-Cl-Ph	I	H
34	2-thienyl	4-Cl-Ph	H	Br
35	2-thienyl	4-Cl-Ph	Cl	H
36	2-thienyl	4-Cl-Ph	Br	H

[a]Reagents and conditions: (a) Toluene/pyridine and rt. The table shows the structural details of the synthesized compounds **24–34**. Compounds **35** and **36** have been reported previously.[17]

https://doi.org/10.1021/acs.jmedchem.0c02163
J. Med. Chem. 2021, 64, 4730–4743

Scheme 4. Synthesis of Amide Bioisosteres of DS2[a]

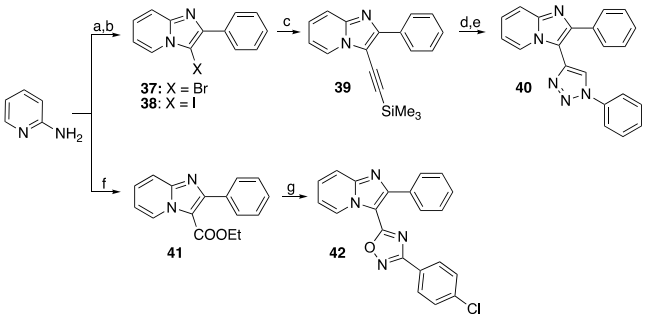

[a]Reagents and conditions: (a) 2-bromo-1-phenylethan-1-one, $NaHCO_3$, MeOH, and reflux; (b) MeCN, NBS for X = Br, NIS for X = I, and rt.; (c) TMSA, $Pd(PPh_3)_2Cl_2$, CuI, Et_3N, and 80 °C; (d) TBAF, THF, and rt.; (e) phenylazide, $CuSO_4{\cdot}5H_2O$, sodium ascorbate, THF/H_2O, and rt.; (f) ethyl 3-oxo-3-phenylpropanoate, CBr_4, MeCN, and 80 °C; (g) 4-chloro-*N*′-hydroxybenzimidamide, DMSO, NaOH, and rt.

substituted 2-aminopyridines, *tert*-butyl isocyanide, and commercially available aliphatic or aromatic aldehydes (Scheme 1). To introduce aromatic moieties into the pyridine ring, the bromide in **1** was used as a handle in a Suzuki−Miyaura cross-coupling reaction with commercially available boronic acids, affording **7** and **8** in decent yield (52−60%). Subsequent acidic deprotection using hydrobromic acid afforded the intermediate amines **10**−**18**.

To expand the flexibility of the design and diversity of the substituents, a complementary strategy was explored based on a key intermediate, **21**, containing a chloride as a handle enabling introduction of an array of substituents in the 2-position of the imidazo[1,2-a]pyridine core scaffold (Scheme 2). The intermediate **21** was synthesized according to procedures reported[35] followed by a Suzuki−Miyaura cross-coupling affording the corresponding 2-phenyl analogue, **22**, in high yield (88%). To explore a broader use of **21** for further structural elaboration, we showed that **21** readily undergoes nucleophilic aromatic substitution with morpholine at room temperature in high yield (not shown).

However, as others before us,[36,37] we encountered difficulties in controlling the apparent substituent-dependent outcome of the reduction of the nitro group. Moreover, the isolation of the resulting amine, under the given reaction conditions, proved complicated. In our hands, using tin(II)-chloride in refluxing methanol proved to be the most feasible method and gave the desired amine **23**.

Finally, the 2-substituted imidazo-[1,2-a]pyridin-3-amides (**24**−**34**) were obtained from the corresponding amines, **10**−**18** and **23**, and the appropriate acyl chlorides in a mixture of toluene and pyridine (Scheme 3). Multiple of the amides proved troublesome to purify using standard column chromatography purification methods. However, classical methods such as trituration or recrystallization afforded the pure target compounds.

The amide bioisosteres, 1,2,3-triazole and 1,2,4-oxadiazole, were obtained as illustrated in Scheme 4. The imidazo[1,2-a]pyridine core scaffold of the intermediates **37** and **38** was synthesized through an initial alkylation−condensation reaction using 2-bromo-1-phenylethan-1-one.

To introduce a handle for the subsequent cross-coupling reaction affording **39**, a regioselective halogenation using *N*-bromo- or *N*-iodosuccinimide was performed to give **37** and **38**, respectively, in high yield.[38] Subsequent Sonogashira cross-

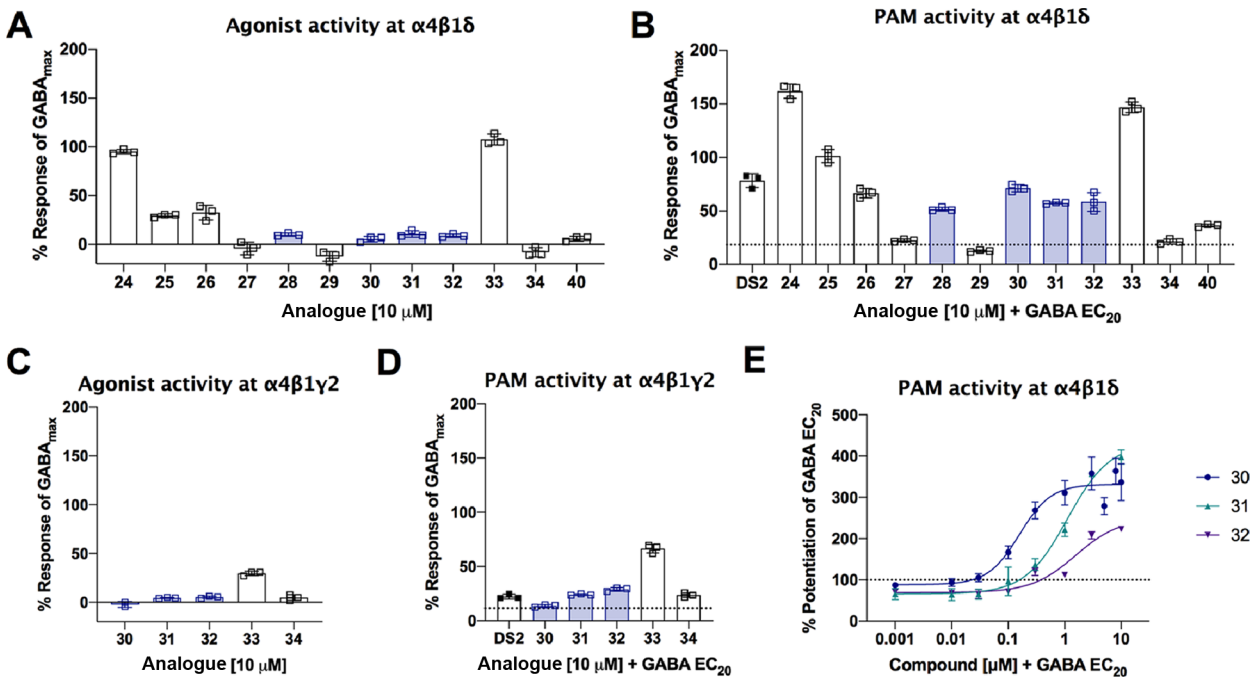

Figure 3. Initial testing of agonists and PAM activity of compounds **24**−**34** and **40** at $\alpha4\beta1\delta$ and compounds **30**−**34** at $\alpha4\beta1\gamma2$ receptors. Agonist activity of 10 μM compounds at (A) $\alpha4\beta1\delta$ and (C) $\alpha4\beta1\gamma2$. PAM activity induced by 10 μM compounds at (B) $\alpha4\beta1\delta$ and (D) $\alpha4\beta1\gamma2$ in the presence of GABA (EC_{20}, see Table 1). (E) Concentration−response curve showing the PAM activity of **30**−**32** at $\alpha4\beta1\delta$. The data are shown as means ± SD. Data in (A), (B), and (E) are representative of two−three independent experiments, and data shown in (C) and (D) are from a single experiment. The dotted line represents the response from GABA EC_{20} coapplied with the analogues, when testing the PAM activity in (B), (D), and (E). Selected compounds investigated further are highlighted in blue.

https://doi.org/10.1021/acs.jmedchem.0c02163
J. Med. Chem. 2021, 64, 4730−4743

coupling followed by a TBAF-mediated deprotection gave access to the terminal alkyne. Interestingly, we found that the bromo analogue, **37**, was superior to the iodo analogue, **38**, as a cross-coupling partner, according to the yield of the compounds obtained, as dehalogenation was observed when using the latter. Finally, the 1,2,3-triazole was installed through a copper-catalyzed alkyne-azide cycloaddition, which furnished **40** in 78% yield.

The ester **41** was prepared as previously described[39] using ethyl 3-oxo-3-phenylpropanoate and subsequent cyclocondensation with 4-chloro-*N*′-hydroxybenzimidamide[40] affording the 1,2,4-oxadiazole **42**.

SAR of the Target Compounds at $\alpha4\beta1\delta$ and $\alpha4\beta1\gamma2$ $GABA_A$Rs. The compounds were subjected to functional characterization in the FMP assay. Initially, the compounds were tested in a single concentration of 10 μM as agonists at $\alpha4\beta1\delta$ and $\alpha4\beta1\gamma2$ $GABA_A$Rs and as PAMs (applied together with a concentration of GABA corresponding to EC_{20}), to evaluate intrinsic activity as well as selectivity (Figure 3).

The compounds **27**, **29**, and **34** were found to have no activity at $\alpha4\beta1\delta$ and were therefore not pursued further. In addition, the poor solubility of the 1,2,4-oxadiazole (**42**) precluded the compound from pharmacological characterization. Compounds **24**−**26** and **33** demonstrated agonist activity as these compounds induced responses at $\alpha4\beta1\delta$ in the absence of GABA, making these compounds ago-PAMs. However, because we were primarily interested in PAMs, these were not characterized further. Instead, compounds **28** and **30**−**32** were singled out as displaying no or limited agonist activity (Figure 3B). The most efficacious of these, **30**−**32**, were further indicated to display some selectivity for $\alpha4\beta1\delta$ over $\alpha4\beta1\gamma2$ (Figure 3D). The bioisosteric replacement of the amide with a triazole was tolerated as **40** revealed PAM activity at $\alpha4\beta1\delta$, although seemingly with a relatively low efficacy.

The two most efficacious agonists, **24** and **33**, in this study display potent modulatory effects as well (Figure 3A,B). However, the SAR obtained for the modulatory effect on GABA activity, in this specific study and described previously,[17] seems to differ from the corresponding SAR for the allosteric agonist effect. This is especially pronounced for the 5-substituted analogues **28** and **30**−**32**, showing a significant modulatory effect but no direct agonist effect.

Next, we generated full concentration−response curves of the 5-methyl, 5-trifluoromethyl, and 5-fluoro DS2 analogues **30**−**32** in the presence of GABA (EC_{20}) (exemplified in Figure 3E, EC_{50} values for **30**−**32** collected in Table 1, and representative raw data in Figure S3). In addition, because of significant structural overlap, we included the previously identified 5-chloro and 5-bromo DS2 analogues, **35** and **36**, in this series as well.[17] The determined EC_{50} values of the PAM activities are shown in Table 1 and representative raw data in Figure S3. The methyl analogue **30** was found to stand out both in terms of potency and selectivity. It displayed a PAM potency of 160 nM (EC_{50}) (Figure 3E), which is approximately 6 times higher than that of DS2 itself at $\alpha4\beta1\delta$. Additionally, **30** showed no activity at 10 μM at $\alpha4\beta1\gamma2$ (>60-fold selectivity for $\alpha4\beta1\delta$). Compounds **35** and **36** were equally potent as **30** but lacked the same degree of selectivity. Compounds **31** and **32** were neither more potent than DS2 itself at $\alpha4\beta1\delta$, nor did they match the selectivity observed for DS2.

Structural Rationalization of Major SAR Observations. The fact that we observe slight potentiation of GABA responses at γ-containing receptors for some of our compounds (Table 1) may seem contradictory to a binding site in the $\alpha_4\delta$ subunit interface. However, considering the possibility of weak binding to a corresponding binding site in an $\alpha1/4\gamma2$S subunit interface, the resulting SAR was still interpreted in reference to our proposed binding model for DS2 in the $\alpha4\delta$ subunit interface (Figure 2). The 5-position (R^3) in the pyridine part of the scaffold (Figure 2C) was investigated in most detail and proved to be important for the δ-selectivity of the compounds. This is evident as **30**−**32**, containing a methyl, trifluoromethyl, or a fluorine at this position, potently potentiated $\alpha4\beta1\delta$ responses, while exhibiting no or negligible activity at $\alpha4\beta1\gamma2$ (Table 1). Surprisingly, the iodinated compound **33,** as the only one of this series, was shown to be a dual allosteric agonist and modulator at both $\alpha4\beta1\delta$ and $\alpha4\beta1\gamma2$ (Figure 3 and Table 1), which is not the typical signature for a ligand binding in the ECD benzodiazepine binding site. Additionally, as demonstrated by the apparently differential effects on potentiation versus activation (Figure 3; **33** vs **30** and **24** vs **25**), the 5-position together with R^2 substituents may be used to optimize the PAM activity over allosteric agonism or vice versa. In contrast to the markedly diminished allosteric agonist effect, the retained PAM activity of **25** with the 4-OPh instead of the 4-Cl in the parent compound, DS2, is consistent with our predicted binding model showing additional available space for substitution (Figure 2B), and this clearly indicates further R^2-substitution possibilities and warrants additional future investigation of other and even bigger and more bulky substituents in this position. For the 5-position (R^3), a five-membered ring seem to be the largest allowed, as the 2-thienyl (**28**) retains PAM activity while a phenyl substituent (**27**) no longer potentiates the GABA EC_{20} response (Figure 3). Again, these results are consistent with our model showing available space at the 5-position (Figure 2A).

Though only a single compound explores R^4 substitution (**34**), the lack of effect with a bromo-substituent in this specific position corroborates with the fairly tight fit between DS2 and the receptor in our model, predicting very limited space for substitution. However, when it comes to the lack of activity for **29** (Figure 3), which has an R^1 phenyl substituent, our model fails to provide an explanation. No apparent specific interactions were obtained in the docking, and there seems

Table 1. PAM Potencies of Selected DS2 Analogues[a]

compound	EC_{50} (μM), [pEC_{50} ± SEM], n			
	$\alpha4\beta1\delta$	$\alpha4\beta1\gamma2$	$\alpha1\beta2\gamma2$	
DS2	0.98	[6.01 ± 0.078], 4	-[d]	-[d]
30	0.16	[6.79 ± 0.082], 4	>10; n = 3[b]	-[d]
31	1.10	[5.96 ± 0.063], 3	n = 2[c]	-[d]
32	1.92	[5.72 ± 0.046], 3	n = 2[c]	-[d]
35	0.14	[6.84 ± 0.140], 5	-[d]	n = 2[c]
36	0.060	[7.22 ± 0.079], 4	-[d]	n = 2[c]

[a]Concentration−response curves were obtained in the FMP assay. Compounds were coapplied with a concentration of GABA corresponding to approximately GABA EC_{20} determined from full GABA concentration−response curves at the respective receptors. Concentrations used to induce EC_{20} response were $\alpha4\beta1\delta$: 0.06 μM, $\alpha4\beta1\gamma2$: 0.6 μM, and $\alpha1\beta2\gamma2$: 0.5 μM. [b]No potentiation in the tested concentration range of 0.01−10 μM. [c]Inactive (potentiation was less than 10% of the GABA max in the tested concentration range of 0.01−10 μM). [d]Not tested.

https://doi.org/10.1021/acs.jmedchem.0c02163
J. Med. Chem. 2021, 64, 4730−4743

to be ample space for the slightly larger phenyl compared to the 2-thienyl. However, it is tempting to speculate from our pharmacological results that this part of the compounds should bind in a tight pocket encompassing a five-membered ring, also nonaromatic (**26**), but no larger than that. On the other hand, compound **40**, which shows moderate PAM activity, has a phenyl in the corresponding position on a scaffold with a triazole bioisostere replacing the amide. Thus, it could also be the common absence of an R^3 substituent that causes the lack of potentiation by **29** and **34**. Further studies are needed to investigate this. Additionally, the triazole bioisoteric replacements of the amide (**40**) conflict with the binding mode of DS2 as it is unable to form both of the charge-assisted hydrogen bonds observed for the amide to α4R135 and δE71, bridging the two subunits across the interface.

Based on the above SAR analysis (summarized in Figure 4), where the pharmacological activity of the majority of the compounds agrees, but a single compound contradicts our binding mode, it remains nonconclusive whether this is the site of action for DS2. To further investigate this hypothesis, structural-guided site-directed mutagenesis studies are currently being analyzed in our lab.

Irrespective of our binding site hypothesis, our novel analogues of DS2 show that the 5-position of the scaffold is clearly vital for the pharmacological profile of the analogues (PAM/ago-PAM) as well as for the preference for $\alpha4\beta1\delta$ versus $\alpha4\beta1\gamma2$. Such dual activity is a known phenomenon,[41] where subtle structural differences result in diverse pharmacological activity profiles and selectivity as previously reported within the cys-loop receptor research field.[42,43]

CONCLUSIONS

In summary, we have synthesized a series of novel DS2 analogues through complementary synthesis strategies allowing structural diversification of the imidazopyridine core scaffold and identified novel compounds with better potency at, and higher selectivity for, δ-containing $GABA_A$Rs. We find that substituents in the 5-position of the imidazopyridine core scaffold severely affect both the δ-selectivity and modulatory activity. Interestingly, the 5-methyl, 5-bromo, and 5-chloro DS2 analogues, **30**, **35,** and **36,** are superior to DS2 at $\alpha4\beta1\delta$ as PAMs with 6- to 16 times increased potency, whereas the structurally closely related 5-iodo analogue, **33**, is an ago-PAM. This illustrates how even small differences in the imidazopyridine core scaffold of DS2 can give rise to diverse pharmacological profiles. Compound **30** provides a useful tool with improved sensitivity and selectivity for studying the specific subtype $\alpha4\beta1\delta$, recently proposed to have a functional role in the hippocampus[44] and possibly toward other δ-containing receptor subtypes.

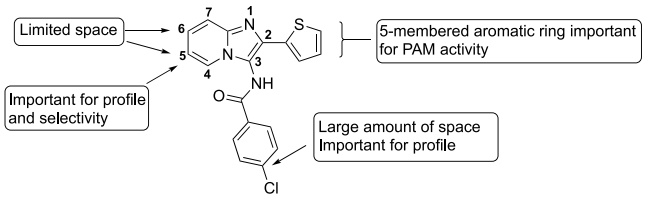

Figure 4. Summarized SAR for the DS2 scaffold in terms of δ-selective allosteric modulation.

EXPERIMENTAL SECTION

Chemistry. *General Procedures.* Melting points (mp) were determined on an SRS OptiMelt apparatus with open capillary tubes. The melting points are uncorrected. Triethylamine was stored over KOH pellets. Thin layer chromatography (TLC) was performed on precoated silica 60 gel F_{254} from Merck and visualized using a UV-lamp at 254/366 nm. Flash column chromatography was conducted manually in glass columns loaded with silica gel 60 (40−63 μm) supplied by Merck. An internal solvent purification system provided anhydrous solvents such as THF, DCM, and DMF. PET refers to the fraction boiling at 40−60 °C. Nuclear magnetic resonance (NMR) spectra were obtained at 300 K on either of two systems. A Bruker Avance II 400 MHz spectrometer equipped with a 5 mm broad band BBFO probe was used. Also, a Bruker Avance III HD 600 MHz spectrometer equipped with a 5 mm cryogenically cooled CPDCH $^{13}C(^1H)$Z-GRD probe was used. 16−64 scans were collected for ^{1}H-NMR spectra, depending on the concentration, with a relaxation delay of 1.0 s. 256−3072 scans were collected for ^{13}C-NMR spectra using a relaxation delay of 2.0 or 4.0 s. The solvent peak was used as the reference in which $CDCl_3$ (7.26 and 77.16 ppm), MeOD-d_4 (3.31 and 49.00 ppm), and DMSO-d_6 (2.50 and 39.52 ppm) were applied, respectively, for ^{1}H- and ^{13}C-NMR. The obtained spectra were processed such as phase- and baseline-corrected in MNova software, version 11.0. The spectral data are reported in the given order: Chemical shift (δ), multiplicity (singlet (s), doublet (d) double doublet (dd), triplet (t), quartet (q), pentet (p), triplet of doublets (td), doublet of doublet of doublets (ddd), broad (b) and multiplet (m)), coupling constant(s) J(Hz), and number of protons. The purity of the final compounds (≥95% unless otherwise stated) was determined on either of two high-performance liquid chromatography (HPLC) systems. The samples were dissolved in 1 mL of (MeCN/H_2O)(1:1) or DMSO in cases in which the solubility of the compounds was found to be insufficient in (MeCN/H_2O)(1:1) and to avoid precipitation of the compounds on the column. HPLC system 1 was a LaChrome reversed phase system from Merck, Germany, Darmstadt that had a Chromolith SpeedROD RP-18 column (4.6 × 50 mm). Detection was performed at 254 nm via an L-7400 UV detector. The samples were injected using an L-7200 auto sampler, injecting 1−10μL. An L7100 pump operating with either a flow rate of 3 or 4 mL/min was used. A linear gradient of A (99.9% H_2O/0.1% TFA) and B (90% MeCN/10% H_2O/0.1% TFA) from 100% A to 90% B over 5 min was applied. The system used EZChromeElite software for data processing and collection. HPLC system 2 was a Dioxnex Ultimate HPLC system, which had an LPG-3400A pump with a flow rate of 1 mL/min, using the previously described mobile phases A and B. A linear gradient system from 100% A to 100% B over 15 min was used. 6 min column equilibration was performed after each run. The column was a Germini-NX C18 column (4.6 × 250 mm, 3μm, 110 Å). A WPS-3000SL auto sampler was used, injecting 1−10 μL. This system had a DAD3000D diode array detector set to 225, 240, 254, and 290 nm. Data processing and collection were conducted using chromeleon software version 6.80. Ultraperformance liquid chromatography-electrospray ionization-mass spectrometry (UPLC-ESI-MS) was performed on an Agilent 1100 HPLC system equipped with a C-18 column (2.1 mm × 50 mm 1.7 μm), which was coupled to a Hewlett Packard 1100 series mass spectrometer with an electrospray ionization source. MassLynx mass spectrometry software version 4.1 was used for data processing. The samples were dissolved in 1 mL of (MeCN/H_2O) (1:1) and filtered through a 0.22 μm filter. The samples were injected via an Acquity FTN Autosampler. A flow rate of 0.8 mL/min was applied. A linear gradient system of A (MeCN/H_2O/HCOOH) (0.05:0.95:0.01) and B (MeCN/HCOOH) (0.99:0.01), which rose from 100% A to 100% B over 3.5 min and then 1 min at 100%, maintaining a flow rate of 0.8 mL/min.

General GBB Procedure for *N*-(*tert*-butyl)-imidazo[1,2-a]-pyridin-3-amine Derivatives. The aldehyde (1 equiv) was dissolved in toluene (40−100 mL). NH_4Cl (1 equiv), *tert*-butyl isocyanide (1.2 equiv), and 2-aminopyridine (1 equiv) were then

https://doi.org/10.1021/acs.jmedchem.0c02163
J. Med. Chem. 2021, 64, 4730−4743

added in that order. The reaction mixture was heated to reflux under argon and monitored by TLC. The reaction mixture was cooled to room temperature, reduced *in vacuo*, and reevaporated with 10 mL toluene to yield the crude product, which was recrystallized to afford the pure *N*-(*tert*-butyl)-imidazo[1,2-*a*]pyridin-3-amines.

***N*-(*tert*-butyl)-6-bromo-2-(thiophen-2-yl)imidazo[1,2-*a*]-pyridin-3-amine (1).** Obtained from 2-thiophenecarboxaldehyde (0.7 mL, 7.1 mmol), NH_4Cl (0.38 g, 7.1 mmol), *tert*-butyl isocyanide (1.0 mL, 8.4 mmol), and 2-amino-5-bromopyridine (1.24 g, 7.1 mmol), using the general GBB procedure. Additional *tert*-Butyl isocyanide (0.2 mL, 1.8 mmol) was added after 18 h. The reaction mixture was refluxed for 48 h in total. The crude product was recrystallized from MeCN/H_2O (16:1). The resulting solid was lyophilized to yield the product as white needles (2.31 g, 93%): mp 184 °C, R_f = 0.5 (DCM : EtOAc) (20 : 1). ^{1}H NMR (400 MHz, Chloroform-*d*) δ 8.34−8.29 (m, 1H), 7.56 (dd, J = 1.0 Hz, 1H), 7.44−7.38 (m, 1H), 7.33 (dd, J = 1.0 Hz, 1H), 7.17 (dd, J = 2.0 Hz, 1H), 7.10 (dd, J = 3.7 Hz, 1H), 3.09 (s, 1H), 1.19 (s, 9H). ^{13}C NMR (151 MHz, Chloroform-*d*) δ 139.68, 136.21, 134.87, 126.80, 126.52, 124.40, 124.25, 122.89, 122.27, 117.04, 105.51, 56.02, 29.70. ESI-MS (m/z) calculated $[M + H]^+$ for $C_{15}H_{16}BrN_3S$ = 350.03, found 350.0 and $[M + H + 2]^+$= 352.0.

***N*-(*tert*-butyl)-6-methyl-2-(thiophen-2-yl)imidazo[1,2-*a*]-pyridin-3-amine (2).**[31] Obtained from 2-thiophenecarboxaldehyde (0.6 mL, 6.0 mmol), NH_4Cl (0.32 g, 6.0 mmol), *tert*-butyl isocyanide (0.8 mL, 7.1 mmol), and 2-amino-5-methylpyridine (0.65 g, 6.0 mmol) using the general GBB procedure. The reaction mixture was refluxed for 23 h. The crude product was recrystallized from MeCN/H_2O (3: 10), which furnished the product as a gray crystalline solid, (1.03 g, 60% yield): mp 193−194 °C. R_f = 0.6 (PET/EtOAc) (1: 1). ^{1}H NMR (400 MHz, Chloroform-*d*) δ 7.98−7.95 (m, 1H), 7.56 (dd, J = 3.6, 1.2 Hz, 1H), 7.42 (dd, J = 9.1, 1.0 Hz, 1H), 7.29 (dd, J = 5.1, 1.2 Hz, 1H), 7.09 (dd, J = 3.6 Hz, 1H), 6.97 (dd, J = 9.1, 1.7 Hz, 1H), 3.06 (s, 1H), 2.33 (s, 3H), 1.18 (s, 9H). ^{13}C NMR (151 MHz, Chloroform-*d*) δ 141.46, 138.02, 134.83, 127.57, 127.37, 124.76, 124.70, 122.77, 121.35, 121.07, 116.73, 56.84, 30.70, 18.57.

***N*-(*tert*-butyl)-2-(thiophen-2-yl)-6-(trifluoromethyl)imidazo-[1,2-a]pyridin-3-amine (3).** Obtained from 2-thiophenecarboxaldehyde (0.9 mL, 9.3 mmol), NH_4Cl, (0.50 g, 9.3 mmol), *tert*-butyl isocyanide (1.3 mL, 11 mmol), and 5-(trifluoromethyl)pyridin-2-amine (1.51 g, 9.3 mmol), using the general GBB procedure. The reaction mixture was refluxed for 41 h. The crude product was recrystallized from MeCN/H_2O (2: 1), which furnished the product as beige to orange needles (2.29 g, 72% yield): mp 153−154 °C. R_f = 0.5 (PET/EtOAc) (2: 1). ^{1}H NMR (400 MHz, Chloroform-*d*) δ 8.61−8.55 (m, 1H), 7.64−7.56 (m, 2H), 7.36 (dd, J = 5.1, 1.1 Hz, 1H), 7.29−7.24 (m, 1H), 7.13 (dd, J = 5.1, 3.6 Hz, 1H), 3.16 (s, 1H), 1.20 (s, 9H). ^{13}C NMR (151 MHz, Chloroform-*d*) δ 141.85, 136.71, 136.65, 127.57, 125.72, 125.63, 123.99, 123.90 (q, J = 270.9 Hz), 122.80 (q, J = 5.8 Hz), 120.29 (q, J = 2.7 Hz), 117.85, 115.97 (q, J = 34.0 Hz), 57.05, 30.63. ^{19}F NMR (376 MHz, Chloroform-*d*) δ −62.08. ESI-MS (m/z) calculated $[M + H]^+$ for $C_{16}H_{17}F_3N_3S$ = 340.11, found 340.1.

***N*-(*tert*-butyl)-6-fluoro-2-(thiophen-2-yl)imidazo[1,2-a]-pyridin-3-amine (4).** Obtained from 2-thiophenecarboxaldehyde (0.9 mL, 9.3 mmol), NH_4Cl, (0.50 g, 9.4 mmol), *tert*-butyl isocyanide (1.3 mL, 11 mmol, 1.2 equiv), and 2-amino-5-fluoropyridine (1.04 g, 9.3 mmol), using the general GBB procedure. The reaction mixture was heated for 37 h. The crude product was recrystallized from MeCN/H_2O (1.2: 1), to furnish the product as beige needles, (1.77 g, 66% yield): mp 188−189 °C. R_f = 0.4 (PET: EtOAc) (2: 1). ^{1}H NMR (400 MHz, Chloroform-*d*) δ 8.12 (dd, J = 4.4, 2.5 Hz, 1H), 7.56 (dd, J = 3.6, 1.1 Hz, 1H), 7.49 (dd, J = 9.7, 5.0 Hz, 1H), 7.33 (dd, J = 5.1, 1.1 Hz, 1H), 7.10 (dd, J = 5.1, 3.6 Hz, 1H), 7.04 (ddd, J = 10.0, 7.8, 2.5 Hz, 1H), 3.10 (s, 1H), 1.19 (s, 9H). ^{13}C NMR (151 MHz, Chloroform-*d*) δ 153.21 (d, J = 236.0 Hz), 139.81, 137.33, 136.48 (d, J = 2.3 Hz), 127.47, 125.24, 125.10, 124.30, 117.78 (d, J = 8.8 Hz), 116.44 (d, J = 25.9 Hz), 110.30 (d, J = 41.5 Hz), 56.97, 30.67. ^{19}F NMR (376 MHz, Chloroform-*d*) δ −140.64 (dt, J = 8.5, 4.8 Hz). ESI-MS (m/z) calculated $[M + H]^+$ for $C_{15}H_{17}FN_3S$ = 290.11, found 290.1.

***N*-(*tert*-butyl)-6-iodo-2-(thiophen-2-yl)imidazo[1,2-a]-pyridin-3-amine (5).** Obtained from 2-thiophenecarboxaldehyde (0.4 mL, 4.3 mmol), NH_4Cl, (0.24 g, 4.5 mmol), *tert*-butyl isocyanide (0.8 mL, 7.2 mmol), and 2-amino-5-iodopyridine[45] (1.00 g, 4.5 mmol), using the general GBB procedure. The reaction mixture was refluxed for 6 h. The crude product was recrystallized from MeCN/H_2O (6: 1), which furnished the product as a white solid (1.18 g, 69% yield): mp 180−181 °C. R_f = 0.7 (PET/EtOAc) (1: 1). ^{1}H NMR (400 MHz, Chloroform-*d*) δ 8.44 (t, J = 1.3 Hz, 1H), 7.59 (d, J = 2.6 Hz, 1H), 7.37−7.28 (m, 3H), 7.11 (dd, J = 5.1, 3.6 Hz, 1H), 3.09 (s, 1H), 1.19 (s, 9H). ^{13}C NMR (151 MHz, Chloroform-*d*) δ 140.73, 137.03, 135.30, 132.30, 128.91, 127.52, 125.43, 125.31, 122.80, 118.37, 74.49, 57.01, 30.70. ESI-MS (m/z) calculated $[M + H]^+$ for $C_{15}H_{17}IN_3S$ = 398.02, found 398.0.

7-bromo-*N*-(*tert*-butyl)-2-(thiophen-2-yl)imidazo[1,2-a]-pyridin-3-amine (6). Obtained from 2-thiophenecarboxaldehyde (0.4 mL, 4.3 mmol), NH_4Cl, (0.23 g, 4.3 mmol), *tert*-butyl isocyanide (0.60 mL, 5.2 mmol), and 2-amino-4-bromopyridine (0.74 g, 4.3 mmol), using the general GBB procedure. The reaction mixture was refluxed for 38 h. The crude product was recrystallized from MeOH/H_2O (10: 1) to furnish the product as off-white needles (0.87 g, 52% yield). This product was slightly contaminated with impurities and was used in the subsequent reaction without further purification. mp 172−173 °C. R_f = 0.5 (PET/EtOAc) (2: 1). ^{1}H NMR (400 MHz, Chloroform-*d*) δ 8.06 (dd, J = 7.3, 0.8 Hz, 1H), 7.70 (s, 1H), 7.57 (d, J = 3.6 Hz, 1H), 7.33 (dd, J = 5.1, 1.1 Hz, 1H), 7.11 (dd, J = 5.1, 3.6 Hz, 1H), 6.85 (dd, J = 7.2, 1.9 Hz, 1H), 3.09 (s, 1H), 1.18 (s, 9H). ESI-MS (m/z) calculated $[M + H +]^+$ for $C_{15}H_{16}BrN_3S$ = 350.03, found 350.0 and $[M + H + 2]^+$= 352.1.

General Suzuki−Miyaura Cross-Coupling Procedure. An aryl halide, such as **1** (1.2 g, 3.4 mmol, 1 equiv), was dissolved in DME (75 mL) and water (38 mL). A boronic acid, such as phenylboronic acid (0.498 g, 4.1 mmol, 1.2 equiv), Na_2CO_3 (0.723 g, 6.8 mmol, 2.0 equiv), and $Pd(PPh_3)_4$ (0.393 g, 0.34 mmol, 10 mol %) were added, respectively. The flask was fitted with a rubber septum and purged with argon. The reaction mixture was then heated to reflux until completion of the reaction monitored by HPLC, cooled to room temperature, and diluted with water (70 mL) and DCM (100 mL). The aqueous layer was extracted with DCM (100 + 200 mL). The combined organic layers were washed with H_2O (110 mL), dried over Na_2SO_4, and reduced *in vacuo*. The crude product was dissolved in DCM, concentrated onto celite, and purified by column chromatography to yield the product and/or purified by recrystallization.

***N*-(*tert*-butyl)-6-phenyl-2-(thiophen-2-yl)imidazo[1,2-*a*]-pyridin-3-amine (7).** Obtained from **1** (1.2 g, 3.4 mmol) and phenylboronic acid (0.498 g, 4.1 mmol), using the general Suzuki−Miyaura cross-coupling procedure. Purification of the crude product was performed by column chromatography (silica gel 60, 40−63 μM) (DCM/EtOAc) (20: 1), which furnished the product as a white solid, (0.62 g, 52% yield): mp 147−148°C. R_f = 0.3 (DCM/EtOAc) (20: 1). R_t = 2.08 min. (4 mL/min flow rate). ^{1}H NMR (400 MHz, Chloroform-*d*) δ 8.38 (dd, J = 1.2 Hz, 1H), 7.63−7.54 (m, 4H), 7.53−7.44 (m, 2H), 7.43−7.37 (m, 2H), 7.32 (dd, J = 5.1, 1.2 Hz, 1H), 7.11 (dd, J = 5.1, 3.6 Hz, 1H), 3.14 (s, 1H), 1.23 (s, 9H).^{13}C NMR (151 MHz, Chloroform-*d*) δ 141.72, 137.96, 137.79, 135.59, 129.25, 127.83, 127.45, 126.97, 125.88, 125.09, 125.02, 124.94, 123.34, 121.02, 117.21, 56.93, 30.79.

***N*-(*tert*-butyl)-2,6-di(thiophen-2-yl)imidazo[1,2-*a*]pyridin-3-amine (8).** Obtained from **1** (0.83 g, 2.4 mmol) and 2-thienylboronic acid (0.37 g, 2.9 mmol), using the general Suzuki−Miyaura cross-coupling procedure. Purification of the crude product was performed by column chromatography (silica gel 60, 40−63 μM) (DCM/MeOH)(40: 1 MeOH). The product was obtained as an off-white solid. The impure fractions containing the product were combined, reduced *in vacuo* and recrystallized from MeCN, and washed with cold MeCN and cold water to yield the product as off-white needles (0.474 g, 60% yield): mp 204−205 °C. R_f = 0.4 (DCM/MeOH)(40: 1). R_t = 2.39 min (3 mL/min flow rate) (>90% pure by HPLC system

https://doi.org/10.1021/acs.jmedchem.0c02163
J. Med. Chem. 2021, 64, 4730−4743

1). ^{1}H NMR (400 MHz, Chloroform-*d*) δ 8.43 (dd, *J* = 1.9, 1.0 Hz, 1H), 7.60 (dd, *J* = 1.0 Hz, 1H), 7.53 (dd, *J* = 9.3, 0.9 Hz, 1H), 7.40 (dd, *J* = 9.3, 1.9 Hz, 1H), 7.32 (ddd, *J* = 7.2, 5.0, 1.1 Hz, 2H), 7.28 (dd, *J* = 3.6, 1.2 Hz, 1H), 7.11 (td, *J* = 3.8 Hz, 2H), 3.13 (s, 1H), 1.23 (s, 9H). ^{13}C NMR (151 MHz, Chloroform-*d*) δ 141.57, 140.85, 137.65, 135.72, 128.33, 127.48, 125.10, 124.99, 124.97, 124.27, 123.73, 123.40, 119.91, 119.89, 117.38, 56.94, 30.81. ESI-MS (m/z) calculated $[M + H]^+$ for $C_{19}H_{20}N_3S_2$ = 354.11, found 354.1.

6-bromo-*N*-(*tert*-butyl)-2-cyclopentylimidazo[1,2-*a*]pyridin-3-amine (9). Obtained from cyclopentanecarbaldehyde (1.0 mL, 9.3 mmol), NH_4Cl, (0.50 g, 9.3 mmol), *tert*-butyl isocyanide (1.3 mL, 11.5 mmol), and 2-amino-5-bromopyridine (1.61 g, 9.3 mmol) using the general GBB procedure. The reaction mixture was refluxed for 46 h. The crude product was recrystallized from MeCN/H_2O (3: 1), which furnished the product as large, slightly gray crystals (2.10 g, 67% yield): mp 143 °C. R_f = 0.6 (PET/EtOAc) (2: 1). ^{1}H NMR (400 MHz, Chloroform-*d*) δ 8.26 (dd, *J* = 1.9, 0.8 Hz, 1H), 7.36 (d, *J* = 9.4 Hz, 1H), 7.11 (dd, *J* = 9.4, 2.0 Hz, 1H), 3.23−3.11 (m, 1H), 2.75 (s, 1H), 2.00−1.90 (m, 6H), 1.76−1.63 (m, 2H), 1.21 (s, 9H).^{13}C NMR (101 MHz, Chloroform-*d*) δ 146.08, 140.70, 126.54, 123.59, 123.35, 117.66, 105.68, 55.39, 37.72, 33.92, 30.48, 26.24. ESI-MS (m/z) calculated $[M + H]^+$ for $C_{16}H_{22}BrN$ = 336.1 found 336.1 and $[M + H + 2]^+$ = 338.2.

General *tert*-Butyl Deprotection Procedure. The *tert*-butyl-protected imidazo[1,2-*a*]pyridin-3-amine was suspended in 10−15 mL of 5 M aqueous HBr. The reaction mixture was heated to 110 °C until completion monitored by HPLC and/or TLC and cooled to room temperature, and the pH of the reaction mixture was adjusted to pH ∼12−14 via aqueous 5 M NaOH. For some compounds, the reaction mixture was cooled in an ice bath during this adjustment of the pH as specified for relevant compounds. The aqueous layer was extracted with EtOAc (3 × 50 mL). The combined organic layers were dried over Na_2SO_4 and subsequently reduced *in vacuo* to yield products as solids. The product was used in the subsequent reaction without further purification unless otherwise specified.

6-bromo-2-(thiophen-2-yl)imidazo[1,2-*a*]pyridin-3-amine (10). Obtained from **1** (0.71 g, 2.0 mmol), using the general *tert*-butyl deprotection procedure and was isolated as a yellow crystalline solid (0.58 g, 98% yield): mp 194−195 °C. R_f = 0.5 (Heptane/EtOAc) (3: 2). R_t = 1.27 min. (4 mL/min flow rate). ^{1}H NMR (400 MHz, Chloroform-*d*) δ 8.16 (dd, *J* = 2.0, 0.9 Hz, 1H), 7.57 (dd, *J* = 3.6, 1.2 Hz, 1H), 7.41 (dd, *J* = 9.4, 0.9 Hz, 1H), 7.35 (dd, *J* = 5.1, 1.1 Hz, 1H), 7.18−7.12 (m, 2H), 3.34 (s, 2H). ^{13}C NMR (151 MHz, Chloroform-*d*) δ 139.76, 136.91, 131.33, 127.93, 127.21, 125.17, 124.16, 122.38, 121.63, 117.98, 106.87. ESI-MS (m/z) calculated $[M + H]^+$ for $C_{11}H_9BrN_3S$ = 293.97, found 293.9 and $[M + H + 2]^+$= 295.9.

6-methyl-2-(thiophen-2-yl)imidazo[1,2-*a*]pyridin-3-amine (11).[46] Obtained from **2** (0.400 g, 1.4 mmol), using the general *tert*-butyl deprotection procedure. Short reaction time (1.5 h) adjustment of pH at 0 °C proved vital. The product was isolated as a yellow crystalline solid (0.319 g, 99% yield): mp = 174−175 °C. R_f = 0.3 (Heptane/EtOAc) (1: 2). R_t = 1.3 min. (4 mL/min flow rate). ^{1}H NMR (400 MHz, Chloroform-*d*) δ 7.79 (t, *J* = 1.6 Hz, 1H), 7.56 (t, *J* = 0.9 Hz, 1H), 7.43 (d, *J* = 9.1 Hz, 1H), 7.31 (dd, *J* = 0.9 Hz, 1H), 7.14 (d, *J* = 3.7 Hz, 1H), 6.96 (d, *J* = 1.6 Hz, 1H), 3.32 (s, 2H), 2.35 (s, 3H). ^{13}C NMR (151 MHz, Chloroform-*d*) δ 140.49, 137.67, 129.92, 127.80, 127.02, 124.48, 123.53, 121.66, 121.32, 119.73, 116.71, 18.52. ESI-MS (m/z) calculated $[M + H]^+$ for $C_{12}H_{11}N_3S$ = 230.7, found 230.5.

2-(thiophen-2-yl)-6-(trifluoromethyl)imidazo[1,2-a]pyridin-3-amine (12). Obtained from **3** (0.47 g, 1.4 mmol) using the general *tert*-butyl deprotection procedure. The reaction mixture was cooled in an ice bath upon adjustment of pH with 5 M NaOH. The product was isolated as a yellow crystalline solid, (0.329 g, 84% yield): mp 208−209 °C. R_f = 0.7 (Heptane/EtOAc) (1: 3). R_t = 8.80 min (>95% pure by HPLC system 2). ^{1}H NMR (400 MHz, Chloroform-*d*) δ 8.46−8.38 (m, 1H), 7.66−7.57 (m, 2H), 7.38 (dd, *J* = 5.1, 1.1 Hz, 1H), 7.29−7.23 (m, 1H), 7.16 (dd, *J* = 5.1, 3.6 Hz, 1H), 3.41 (s, 2H). ^{13}C NMR (151 MHz, DMSO-d_6) δ 137.90, 137.72, 128.00, 127.21, 124.53 (q, *J* = 270.9 Hz), 124.27, 123.90, 122.51, 122.13 (q, *J* = 5.9 Hz), 117.16, 116.60 (q, *J* = 2.6 Hz), 113.76 (q, *J* = 33.1 Hz). ^{19}F NMR (376 MHz, DMSO-d_6) δ −60.43. ESI-MS (m/z) calculated $[M + H]^+$ for $C_{12}H_9F_3N_3S$ = 284.05, found 284.0.

6-fluoro-2-(thiophen-2-yl)imidazo[1,2-a]pyridin-3-amine (13). Obtained from **4** (0.40 g, 1.4 mmol) using the general *tert*-butyl deprotection procedure. The reaction mixture was cooled in an ice bath upon adjustment of pH with 5 M NaOH. The product was isolated as a greenish crystalline solid (0.278 g, 85% yield): mp 201−202 °C (decomp.). R_f = 0.6 (PET/EtOAc) (1: 3) + 1% Et_3N. ^{1}H NMR (400 MHz, Chloroform-*d*) δ 7.96−7.93 (m, 1H), 7.56 (dd, *J* = 3.7, 1.1 Hz, 1H), 7.51−7.45 (m, 1H), 7.34 (dd, *J* = 5.1, 1.1 Hz, 1H), 7.14 (dd, *J* = 5.1, 3.6 Hz, 1H), 7.02 (ddd, *J* = 10.1, 8.0, 2.4 Hz, 1H), 3.33 (s, 2H). ^{13}C NMR (151 MHz, Chloroform-*d*) δ 153.52 (d, *J* = 236.4 Hz), 138.95, 137.14, 132.00 (d, *J* = 2.0 Hz), 127.88, 124.96, 123.89, 122.71, 117.83 (d, *J* = 8.9 Hz), 115.76 (d, *J* = 25.9 Hz), 108.74 (d, *J* = 41.4 Hz). ^{19}F NMR (376 MHz, Chloroform-*d*) δ −140.25 (q, *J* = 5.4 Hz). ESI-MS (m/z) calculated $[M + H]^+$ for $C_{11}H_9FN_3S$ = 234.05, found 234.0.

6-iodo-2-(thiophen-2-yl)imidazo[1,2-a]pyridin-3-amine (14). Obtained from **5** (0.450 g, 1.1 mmol) using the general *tert*-butyl deprotection procedure. The reaction mixture was cooled in an ice bath upon adjustment of pH with 5 M NaOH. The product was isolated as a yellow crystalline solid (0.322 g, 83% yield). R_f = 0.7 (Heptane/EtOAc) (1: 3) + 1% Et_3N.^{1}H NMR (400 MHz, Chloroform-*d*) δ 8.34−8.25 (m, 1H), 7.57 (dd, *J* = 3.6, 1.1 Hz, 1H), 7.35 (dd, *J* = 5.1, 1.1 Hz, 1H), 7.33−7.27 (m, 2H), 7.14 (dd, *J* = 5.1, 3.6 Hz, 1H), 3.33 (s, 2H). ^{13}C NMR (151 MHz, DMSO-d_6) δ 138.20, 136.83, 128.88, 127.90, 126.93, 125.53, 123.92, 123.13, 122.12, 117.54, 74.89.ESI-MS (m/z) calculated $[M + H]^+$ for $C_{11}H_9IN_3S$ = 341.96, found 341.9.

7-bromo-2-(thiophen-2-yl)imidazo[1,2-a]pyridin-3-amine (15). Obtained from **6** (0.40 g, 1.2 mmol,1 equiv) using the general *tert*-butyl deprotection procedure. The reaction mixture was cooled in an ice bath upon adjustment of pH with 5 M NaOH. The product was isolated as an orange solid (0.313 g, 87% yield). This product was used in the subsequent reactions without further purification. R_f = 0.6 (PET/EtOAc) (1: 1.5). ^{1}H NMR (400 MHz, Chloroform-*d*) δ 7.91 (d, *J* = 7.2 Hz, 1H), 7.72 (s, 1H), 7.59 (d, *J* = 3.6 Hz, 1H), 7.36 (dd, *J* = 5.1, 1.1 Hz, 1H), 7.15 (dd, *J* = 5.1, 3.6 Hz, 1H), 6.92 (dd, *J* = 7.2, 1.8 Hz, 1H), 3.35 (s, 2H). ESI-MS (m/z) calculated $[M + H]^+$ for $C_{11}H_9BrN_3S$ = 293.97, found 293.9 and $[M + H + 2]^+$= 295.9.

6-phenyl-2-(thiophen-2-yl)imidazo[1,2-*a*]pyridin-3-amine (16). Obtained from **7** (0.56 g, 1.6 mmol, 1 equiv) and 5 M aq. HBr (70 mL), using the general *tert*-butyl deprotection procedure. The product was isolated as a yellow solid (0.435 g, 92% yield): mp 189−191 °C. R_f = 0.7 (PET/EtOAc) (1: 3). ^{1}H NMR (600 MHz, Chloroform-*d*) δ 8.21 (dd, *J* = 1.9, 1.0 Hz, 1H), 7.64−7.57 (m, 4H), 7.48 (dd, *J* = 8.5, 6.9 Hz, 2H), 7.42−7.39 (m, 2H), 7.35 (dd, *J* = 5.1, 1.1 Hz, 1H), 7.16 (dd, *J* = 5.1, 3.6 Hz, 1H), 3.39 (s, 2H). ^{13}C NMR (151 MHz, Chloroform-*d*) δ 140.71, 137.76, 137.43, 130.71, 129.22, 127.91, 127.85, 127.00, 126.40, 124.74, 124.55, 123.78, 121.91, 119.36, 117.10. ESI-MS (m/z) calculated $[M + H]^+$ for $C_{17}H_{14}N_3S$ = 292.09, found 292.1.

2,6-di(thiophen-2-yl)imidazo[1,2-*a*]pyridin-3-amine (17). Obtained from **8** (0.110 g, 0.30 mmol 1 equiv) using the general *tert*-butyl deprotection procedure, 5 M aq. HBr (26 mL) and was isolated as a yellow crystalline solid (0.087 g, 94% yield): mp 197−198 °C. R_f = 0.6 (PET/EtOAc) (1: 3). R_t = 1.95 min (3 mL/min).^{1}H NMR (400 MHz, Chloroform-*d*) δ 8.23 (dd, *J* = 1.8, 1.0 Hz, 1H), 7.59 (dd, *J* = 3.6, 1.0 Hz, 1H), 7.54 (dd, *J* = 9.3, 1.0 Hz, 1H), 7.38 (dd, *J* = 9.3, 1.9 Hz, 1H), 7.35−7.29 (m, 3H), 7.15 (dd, *J* = 5.1, 3.6 Hz, 1H), 7.12 (dd, *J* = 5.1, 3.6 Hz, 1H), 3.38 (s, 2H). ^{13}C NMR (151 MHz, Chloroform-*d*) δ 140.62, 140.58, 137.33, 130.93, 128.30, 127.87, 125.10, 124.83, 123.88, 123.84, 123.75, 121.93, 120.40, 118.16, 117.28. ESI-MS (m/z) calculated $[M + H]^+$ for $C_{15}H_{11}N_3S_2$ = 298.05, found 298.0.

6-bromo-2-cyclopentylimidazo[1,2-*a*]pyridin-3-amine (18). Obtained from **9** (0.242 g, 0.7 mmol, 1 equiv) using the general *tert*-butyl deprotection procedure. The extraction was performed with

https://doi.org/10.1021/acs.jmedchem.0c02163
J. Med. Chem. 2021, 64, 4730−4743

EtOAc (2 × 200 mL) and once with a mixture of MeOH (30 mL) in EtOAc (200 mL) to obtain complete extraction of the product. The compound was isolated as an orange solid (0.196 g, 100% yield). R_f = 0.5 (Heptane/EtOAc) (1: 3) + 1% Et_3N. R_t = 1.57 (3 mL/min flow rate). ^1H NMR (400 MHz, Chloroform-*d*) δ 8.14 (dd, J = 2.0, 0.9 Hz, 1H), 7.37 (dd, J = 9.4, 0.9 Hz, 1H), 7.09 (dd, J = 9.5, 1.9 Hz, 1H), 3.28−3.16 (m, 1H), 3.00 (s, 2H), 2.07−2.00 (m, 2H), 1.96−1.81 (m, 4H), 1.75−1.66 (m, 2H). ^{13}C NMR (101 MHz, Chloroform-*d*) δ 141.41, 139.35, 125.75, 122.13, 121.80, 117.65, 106.19, 37.72, 33.04, 25.99. ESI-MS (m/z) calculated $[M + H]^+$ for $C_{12}H_{14}BrN_3$ = 280.04, found 280.0 and $[M + H + 2]^+$ = 282.0.

3-nitro-2-phenylimidazo[1,2-*a*]pyridine (22).[47] Obtained from **21**[35] (0.500 g, 2.5 mmol), phenyl boronic acid (0.370 g, 3.0 mmol), Na_2CO_3 (0.268 g, 2.5 mmol, 1 equiv), and $Pd(PPh_3)_4$ (0.288 g, 0.25 mmol, 10 mol %) using the general Suzuki−Miyaura cross-coupling procedure. The crude product was dissolved in DCM, concentrated onto silica gel 60 (40−63 μm), and subsequently purified by column chromatography (EtOAc/Heptane) (1: 1) to furnish the product as a yellow solid (0.525 g, 88% yield). ^1H NMR (400 MHz, Chloroform-*d*) δ 9.52 (dt, J = 7.1, 1.2 Hz, 1H), 7.96−7.87 (m, 2H), 7.85 (dt, J = 8.9, 1.1 Hz, 1H), 7.66 (ddd, J = 8.9, 7.0, 1.3 Hz, 1H), 7.57−7.47 (m, 3H), 7.29 (td, J = 7.0, 1.3 Hz, 1H). ^{13}C NMR (151 MHz, Chloroform-*d*) δ 150.42, 145.29, 132.02, 130.98, 130.33, 130.18, 129.10, 128.32, 128.28, 118.46, 116.61. The spectral data were consistent with previously reported data.[47]

2-phenylimidazo[1,2-*a*]pyridin-3-amine (23).[34] **22** (1.00 g, 4.2 mmol) was dissolved in MeOH (39 mL) and then $SnCl_2$ (3.98 g, 20.0 mmol) was added. The reaction mixture was stirred overnight at reflux (65 °C). The reaction mixture was then cooled to room temperature, and the solvent was removed *in vacuo*. A small amount of EtOAc was then added, and the pH of the solution was adjusted with 5 M aqueous NaOH to pH∼7. The reaction mixture was left stirring for 2 h. Additional EtOAc was added, and the solution was filtered through celite. The compound was then extracted through continuous extraction overnight using EtOAc and reduced *in vacuo* to obtain the product as a white solid (0.740 g, 83% yield). ^1H NMR (400 MHz, Chloroform-*d*) δ 8.04−7.94 (m, 3H), 7.55 (dt, J = 9.1, 1.1 Hz, 1H), 7.47 (dd, J = 8.4, 7.0 Hz, 2H), 7.37−7.28 (m, 1H), 7.11 (ddd, J = 9.1, 6.7, 1.3 Hz, 1H), 6.81 (td, J = 6.7, 1.1 Hz, 1H), 3.40 (s, 2H).^{13}C NMR (151 MHz, Methanol-d_4) δ 141.62, 135.56, 130.66, 129.60, 128.16, 127.91, 126.69, 124.67, 123.53, 116.95, 112.92. The spectral data in Chloroform-*d* were consistent with previously reported data.[34]

General Acylation Procedure for the Synthesis of Imidazo-[1,2-a]Pyridine Benzamides. Flame- or oven-dried glassware was used. The imidazo[1,2-*a*]pyridine-3-amines (0.5 mmol, 1 equiv) were suspended in dry toluene (3 mL) and dry pyridine (1 mL). The flask was fitted with a rubber septum and purged with argon. The acyl chloride (1.2 equiv) was added at once through the septum, and the reaction mixture was stirred at room temperature and monitored by TLC, UPLC-ESI-MS, and/or HPLC. The crude product was obtained and purified as specified.

***N*-(6-bromo-2-(thiophen-2-yl)imidazo[1,2-*a*]pyridin-3-yl)-benzamide (24).** Obtained from **10** (0.145 g, 0.5 mmol) and benzoyl chloride (0.07 mL, 0.6 mmol) using the general acylation procedure for imidazo[1,2-*a*]pyridine benzamides. The crude product was obtained by adding 1.5 mL of water to the reaction mixture, which was subsequently stirred for 30 min. The reaction mixture was cooled in an ice bath, and the precipitate was collected by filtration and washed with cold water (5 °C, 3 × 3 mL) and cold acetone (−18 °C, 3 mL) to yield the crude product. The crude product was recrystallized from toluene, which furnished the product as a white solid: mp 269 °C. R_f = 0.4 (DCM: EtOAc) (5: 1). R_t = 1.58 min (4 mL/min flow rate) (>95% pure by HPLC system 1). ^1H NMR (400 MHz, Methanol-d_4) δ 8.27 (t, J = 1.3 Hz, 1H), 8.19−8.12 (m, 2H), 7.74−7.65 (m, 1H), 7.65−7.57 (m, 3H), 7.55−7.45 (m, 3H), 7.13 (dd, J = 5.1, 3.7 Hz, 1H). ^{13}C NMR (151 MHz, Methanol-d_4) δ 170.17, 142.95, 136.78, 135.80, 134.03, 134.00, 130.84, 129.97, 129.27, 128.69, 127.56, 126.73, 124.85, 118.23, 115.98, 108.66. ESI-MS (m/z) calculated $[M + H]^+$ for $C_{18}H_{12}BrN_3OS$ = 398.00, found 398.5 and $[M + H + 2]^+$ = 400.5.

***N*-(6-bromo-2-(thiophen-2-yl)imidazo[1,2-*a*]pyridin-3-yl)-4-phenoxybenzamide (25).** Obtained from **10** (0.140 g, 0.50 mmol) and 4-phenoxybenzoyl chloride (0.140 g, 0.6 mmol) using the general acylation procedure for imidazo[1,2-a]pyridine benzamides. The reaction mixture was reduced *in vacuo,* and the resulting solid was washed with cold H_2O and cold acetone and dried *in vacuo*. The product was purified by trituration from MeOH and subsequently washed with H_2O and MeOH and dried under high vacuum. The product was isolated as a white solid (0.047 g, 20% yield): mp 266 °C. R_f = 0.6 (PET/EtOAc) (1: 2) + 1% Et_3N. R_t = 2.35 min (3 mL/min flow rate) (>99% pure by HPLC system 1). ^1H NMR (400 MHz, DMSO-d_6) δ 10.59 (s, 1H), 8.53 (d, J = 2.3 Hz, 1H), 8.21−8.13 (m, 2H), 7.64−7.54 (m, 2H), 7.51−7.42 (m, 4H), 7.28−7.23 (m, 1H), 7.22−7.10 (m, 5H). ^{13}C NMR (151 MHz, DMSO-d_6) δ 165.89, 160.50, 155.39, 140.52, 135.67, 134.80, 130.55, 130.33, 128.45, 127.92, 127.52, 126.55, 124.78, 124.55, 123.94, 119.72, 117.68, 117.44, 115.03, 106.48. ESI-MS (m/z) calculated $[M + H]^+$ for $C_{24}H_{16}BrN_3O_2S$ = 490.0, found 490.0 and $[M + H + 2]^+$= 492.0.

***N*-(6-bromo-2-cyclopentylimidazo[1,2-*a*]pyridin-3-yl)-benzamide (26).** Obtained from **18** (0.223 g, 0.8 mmol) and benzoyl chloride (0.1 mL, 1.1 mmol) using the general acylation procedure for imidazo[1,2-a]pyridine benzamides. No precipitate formed upon addition of 1.5 mL of water to the reaction mixture. The reaction mixture was reduced *in vacuo* and then concentrated on celite and purified by column chromatography (silica gel 60, 40−63 μM) (DCM/MeOH/Et_3N) (20: 0.5: 0.01). Selected pure fractions were combined and reduced, and the resulting product was then triturated from MeCN, reduced *in vacuo,* then under high vacuum, and finally lyophilized to yield the product as a white solid (0.012 g, 4% yield). R_f = 0.5 (DCM/MeOH) (40: 1) + 1% Et_3N. R_t = 10.40 min (>99% pure by HPLC system 2). ^1H NMR (400 MHz, DMSO-d_6) δ 10.30 (s, 1H), 8.35 (d, J = 1.9 Hz, 1H), 8.11−8.04 (m, 2H), 7.70−7.61 (m, 1H), 7.57 (dd, J = 8.4, 6.8 Hz, 2H), 7.52 (d, J = 9.5 Hz, 1H), 7.34 (dd, J = 9.5, 1.9 Hz, 1H), 3.14 (p, J = 8.1 Hz, 1H), 1.94 (dtd, J = 10.7, 6.6, 5.2, 2.7 Hz, 2H), 1.83−1.71 (m, 4H), 1.60 (dt, J = 8.6, 4.7 Hz, 2H). ^{13}C NMR (151 MHz, DMSO-d_6) δ 166.51, 145.55, 139.96, 133.12, 132.12, 128.45, 128.08, 126.61, 123.41, 117.58, 115.66, 105.51, 37.06, 32.28, 25.34. ESI-MS (m/z) calculated $[M + H]^+$ for $C_{19}H_{18}BrN_3O$ = 384.07, found 384.1 and $[M + H + 2]^+$ = 386.0.

***N*-(6-phenyl-2-(thiophen-2-yl)imidazo[1,2-*a*]pyridin-3-yl)-benzamide (27).** Obtained from **16** (0.150 g, 0.5 mmol) and benzoyl chloride (0.07 mL, 0.6 mmol) using the general acylation procedure for imidazo[1,2-a]pyridine benzamides. The reaction mixture was reduced *in vacuo,* and the resulting solid was recrystallized from THF to yield the product as a white solid (0.034 g, 17% yield): mp 270−271°C. R_f = 0.4 (PET/EtOAc) (1: 3). R_t = 11.37 min. (>95% pure by HPLC system 2). ^1H NMR (600 MHz, Methanol-d_4) δ 8.76 (t, J = 1.4 Hz, 1H), 8.36 (dd, J = 9.3, 1.7 Hz, 1H), 8.19 (d, J = 7.4 Hz, 2H), 8.04 (d, J = 1.0 Hz, 1H), 7.80 (ddd, J = 12.5, 4.4, 1.1 Hz, 2H), 7.76−7.70 (m, 3H), 7.64 (t, J = 7.8 Hz, 2H), 7.54 (dd, J = 8.3, 6.6 Hz, 2H), 7.52−7.45 (m, 1H), 7.29 (t, J = 3.9 Hz, 1H). ^{13}C NMR (151 MHz, Methanol-d_4) δ 170.42, 139.02, 136.17, 135.73, 134.46, 133.58, 133.39, 131.42, 130.54, 130.40, 130.05, 129.74, 129.53, 129.30, 128.65, 128.55, 127.71, 123.58, 117.88, 113.17. ESI-MS (m/z) calculated $[M + H]^+$ for $C_{24}H_{17}N_3OS$ = 396.12, found 396.2 and 397.2.

***N*-(2,6-di(thiophen-2-yl)imidazo[1,2-*a*]pyridin-3-yl)-benzamide (28).** Obtained from **17** (0.23 g, 0.9 mmol) and benzoyl chloride (0.1 mL 1.0 mmol) using the general acylation procedure for imidazo[1,2-a]pyridine benzamides. The crude product was obtained by adding 0.5 mL of water to the reaction mixture and stirred for 30 min. The reaction mixture was cooled in an ice bath, and the precipitate was collected by filtration and washed with cold water to yield the crude product (0.247 g). 0.125 g of the crude product was recrystallized from EtOH, then dried *in vacuo,* and finally dried under high vacuum. The product was isolated as a white solid (0.038 g, 32% yield): mp 253 °C. R_f = 0.3 (DCM/ MeOH) (40: 1) + 1% Et_3N. R_t = 11.27 min (>99% pure by HPLC system 2). ^1H NMR (400 MHz,

https://doi.org/10.1021/acs.jmedchem.0c02163
J. Med. Chem. 2021, 64, 4730−4743

DMSO-d_6) δ 10.67 (s, 1H), 8.35 (d, J = 1.6 Hz, 1H), 8.20−8.13 (m, 2H), 7.75−7.55 (m, 8H), 7.51 (d, J = 3.6 Hz, 1H), 7.15 (ddd, J = 8.6, 5.1, 3.6 Hz, 2H). ^{13}C NMR (151 MHz, DMSO-d_6) δ 166.70, 141.27, 139.14, 136.08, 134.80, 133.04, 132.38, 128.66, 128.50, 128.13, 127.88, 126.29, 126.02, 124.90, 124.76, 124.52, 119.97, 118.98, 117.06, 115.01. ESI-MS (m/z) calculated $[M + H]^+$ for $C_{22}H_{15}N_3OS_2$ = 402.07, found 402.1.

***N*-(2-phenylimidazo[1,2-*a*]pyridin-3-yl)benzamide (29).**[48] Benzoyl chloride (0.141 g, 1.0 mmol) in DCM (0.7 mL) was slowly added to the stirring solution of DIPEA (0.174 g, 1.35 mmol) and **23** (0.15 g, 0.7 mmol) in DCM at 0 °C. The reaction mixture was left stirring for 3 h at room temperature and monitored by TLC. The reaction mixture was reduced *in vacuo,* and the resulting product was purified by column chromatography (EtOAc/Heptane) (6: 4) + 1% Et_3N to furnish the product as a white solid (0.117 g, 52% yield): mp 214−215 °C. R_t = 1.77 min (94% pure by HPLC system 1). ^{1}H NMR (600 MHz, DMSO-d_6) δ 10.71 (s, 1H), 8.12 (ddt, J = 8.2, 6.9, 1.2 Hz, 3H), 8.03−7.91 (m, 2H), 7.77−7.59 (m, 4H), 7.51−7.40 (m, 2H), 7.37−7.30 (m, 2H), 6.96 (td, J = 6.7, 1.1 Hz, 1H).^{13}C NMR (151 MHz, DMSO-d_6) δ 166.70, 142.08, 137.83, 133.59, 132.98, 132.36, 128.68, 128.55, 128.00, 127.68, 126.63, 125.20, 123.77, 116.92, 115.44, 112.24. ESI-MS (m/z) calculated $[M + H]^+$ for $C_{20}H_{16}N_3O$ = 314.13, found 314.1.

4-chloro-*N*-(6-methyl-2-(thiophen-2-yl)imidazo[1,2-*a*]-pyridin-3-yl)benzamide (30). Obtained from **11** (0.130 g, 0.57 mmol) and 4-chlorobenzoyl chloride (0.090 mL 0.70 mmol, 1.2 equiv) using the general acylation procedure for imidazo[1,2-a]pyridine benzamides. The crude product was obtained by adding 0.9 mL of distilled water to the reaction mixture and stirred at 0 °C for 30 min. The precipitating white solid was collected by filtration and washed with water and recrystallized from EtOAc. Filtration and drying *in vacuo* and freeze drying furnished the product as a white crystalline solid (0.095 g, 46% yield): mp = 276 °C. R_f = 0.2 (Heptane/EtOAc) (1: 2) + 1% Et_3N. R_t = 10.61 min (>98% pure by HPLC system 2). ^{1}H NMR (400 MHz, DMSO-d_6) δ 10.67 (s, 1H), 8.19−8.12 (m, 2H), 8.03−7.98 (m, 1H), 7.74−7.66 (m, 2H), 7.53 (dt, J = 6.8, 1.6 Hz, 2H), 7.45 (dd, J = 3.7, 1.2 Hz, 1H), 7.21 (dd, J = 9.2, 1.7 Hz, 1H), 7.11 (dd, J = 5.1, 3.6 Hz, 1H), 2.30 (s, 3H). ^{13}C NMR (151 MHz, DMSO-d_6) δ 165.67, 141.12, 137.25, 136.26, 133.84, 131.80, 130.01, 128.74, 128.56, 127.79, 125.94, 124.15, 121.91, 121.19, 115.97, 113.82, 17.52. ESI m/z calculated $[M + H]^+$ for $C_{19}H_{15}ClN_3OS$ = 368.06, found 368.1 and $[M + H + 2]^+$ 370.1.

4-chloro-*N*-(2-(thiophen-2-yl)-6-(trifluoromethyl)imidazo-[1,2-a]pyridin-3-yl)benzamide (31). Obtained from **12** (0.166 g, 0.59 mmol) and 4-chlorobenzoyl chloride (0.090 mL 0.70 mmol) using the general acylation procedure for imidazo[1,2-a]pyridine benzamides. The crude product was obtained by adding 1 mL of water to the reaction mixture and stirred at 0 °C for 30 min. The precipitated solid was collected by filtration and washed with water and then dried *in vacuo*. To the filtrate was added water (15 mL), and this aqueous layer was extracted with DCM (2 × 15 mL). The combined organic layers were dried over Na_2SO_4, combined with the initially collected precipitate, and reduced *in vacuo* to furnish the crude product. The crude product was concentrated on celite and purified by column chromatography (silica gel 60, 40−63 μM) (Heptane/EtOAc) (1: 0.9), reduced under high vacuum, and freeze-dried. The product was isolated as a white solid (0.034 g, 14% yield): mp 268 °C. R_f = 0.4 (Heptane/EtOAc) (1: 0.9). R_t = 12.89 min (>99% pure by HPLC system 2).^{1}H NMR (400 MHz, DMSO-d_6) δ 10.79 (s, 1H), 8.93−8.82 (m, 1H), 8.23−8.09 (m, 2H), 7.83 (d, J = 9.4 Hz, 1H), 7.75−7.68 (m, 2H), 7.63−7.56 (m, 2H), 7.54 (dd, J = 3.6, 1.2 Hz, 1H), 7.15 (dd, J = 5.1, 3.6 Hz, 1H). ^{13}C NMR (151 MHz, DMSO-d_6) δ 165.81, 141.92, 137.29, 135.84, 135.26, 131.77, 130.18, 128.66, 128.01, 127.03, 125.31, 123.87 (q, J = 5.5 Hz), 121.14 (q, J = 271.3 Hz), 120.90 (q, J = 3.3, 2.0 Hz), 117.66, 115.83, 115.07 (q, J = 33.6 Hz). ^{19}F NMR (376 MHz, DMSO-d_6) δ −59.90. ESI m/z calculated $[M + H]^+$ for $C_{19}H_{12}ClF_3N_3OS$ = 422.03, found 422.1 and $[M + H + 2]^+$= 424.1.

4-chloro-N-(6-fluoro-2-(thiophen-2-yl)imidazo[1,2-a]-pyridin-3-yl)benzamide (32). Obtained from **13** (0.210 g, 0.9 mmol) and 4-chlorobenzoyl chloride (0.1 mL 0.8 mmol) using the general acylation procedure for imidazo[1,2-a]pyridine benzamides. The crude product was obtained by adding 1.5 mL of water to the reaction mixture and stirred at 0 °C for 30 min. The precipitating solid was collected by filtration and washed with water and dried *in vacuo* to yield the crude product. The crude product was triturated from EtOAc(15 mL), purified by recrystallizations, first from EtOAc (15 mL) and then from MeOH (14 mL), and dried *in vacuo* to furnish the product as a white solid (0.052 g, 16% yield): mp 289 °C. R_f = 0.4 (PET/EtOAc) (2: 1). R_t = 10.73 min (>99% pure by HPLC system 2). ^{1}H NMR (400 MHz, DMSO-d_6) δ 10.73 (s, 1H), 8.51 (dd, J = 4.5, 2.4 Hz, 1H), 8.18−8.11 (m, 2H), 7.73−7.65 (m, 3H), 7.56 (dd, J = 5.1, 1.2 Hz, 1H), 7.48 (dd, J = 3.7, 1.2 Hz, 1H), 7.42 (ddd, J = 10.1, 8.3, 2.5 Hz, 1H), 7.13 (dd, J = 5.1, 3.6 Hz, 1H). ^{13}C NMR (151 MHz, DMSO-d_6) δ 165.66, 152.88 (d, J = 233.8 Hz), 139.86, 137.22, 135.90, 135.46 (d, J = 2.1 Hz), 131.82, 130.10, 128.66, 127.89, 126.32, 124.53, 117.47 (d, J = 9.1 Hz), 117.14 (d, J = 25.8 Hz), 115.71 (d, J = 1.9 Hz), 111.09 (d, J = 41.8 Hz). ^{19}F NMR (376 MHz, DMSO-d_6) δ −140.31 (dt, J = 9.2, 4.8 Hz). ESI m/z calculated $[M + H]^+$ for $C_{18}H_{12}ClFN_3OS$ = 372.04, found 372.0 and $[M + H + 2]^+$ = 374.1.

4-chloro-*N*-(6-iodo-2-(thiophen-2-yl)imidazo[1,2-a]pyridin-3-yl)benzamide (33). Obtained from **14** (0.272 g, 0.8 mmol) and 4-chloro benzoyl chloride (0.159 g, 0.9 mmol) using the general acylation procedure for imidazo[1,2-a]pyridine benzamides. The crude product was obtained by adding water (1.5 mL) to the reaction mixture, which was then cooled in an ice bath for 30 min. The precipitate was collected by filtration, washed with water, and dried *in vacuo* to yield the crude product. Recrystallization from MeOH (26 mL) and drying *in vacuo* furnish the product as white needles (0.087 g, 23% yield): mp 279−280 °C. R_f = 0.5 (Heptane/EtOAc) (1: 2). R_t = 11.55 min (>99% pure by HPLC system 2). ^{1}H NMR (400 MHz, DMSO-d_6) δ 10.68 (s, 1H), 8.59 (d, J = 1.5 Hz, 1H), 8.18−8.10 (m, 2H), 7.70 (d, J = 8.5 Hz, 2H), 7.59−7.50 (m, 2H), 7.50−7.42 (m, 2H), 7.12 (dd, J = 5.1, 3.6 Hz, 1H). ^{13}C NMR (151 MHz, DMSO-d_6) δ 165.75, 140.74, 137.22, 135.66, 134.36, 133.12, 131.81, 130.13, 128.64, 128.37, 127.90, 126.49, 124.73, 117.88, 114.06, 76.49. ESI m/z calculated $[M + H]^+$ for $C_{18}H_{11}ClIN_3OS$ = 479.94, found 480.0 and $[M + H + 2]^+$ = 482.0.

***N*-(7-bromo-2-(thiophen-2-yl)imidazo[1,2-a]pyridin-3-yl)-4-chlorobenzamide (34).** Obtained from **15** (0.216 g, 0.7 mmol) and 4-chlorobenzoyl chloride (0.129 g, 0.7 mmol) using the general acylation procedure for imidazo[1,2-a]pyridine benzamides. The crude product was obtained by adding water (2 mL) to the reaction mixture, which was then cooled in an ice bath for 30 min. The precipitate was collected by filtration, washed with water, and dried *in vacuo* to yield the crude product. Recrystallization from MeOH (14 mL) and drying *in vacuo* with Et_2O (5 mL) added twice were performed, which furnished the product as white needles (0.071 g, 23% yield): mp 266 °C. R_f = 0.6 (Heptane/EtOAc) (1: 1). R_t = 11.41 min (>95% pure by HPLC system 2). ^{1}H NMR (400 MHz, DMSO-d_6) δ 10.77 (s, 1H), 8.18 (d, J = 7.2 Hz, 1H), 8.14 (d, J = 8.6 Hz, 2H), 7.96 (d, J = 1.8 Hz, 1H), 7.75−7.65 (m, 2H), 7.58 (dd, J = 5.1, 1.2 Hz, 1H), 7.50 (dd, J = 3.6, 1.2 Hz, 1H), 7.19−7.08 (m, 2H). ^{13}C NMR (151 MHz, DMSO-d_6) δ 165.68, 142.21, 137.34, 135.60, 134.69, 131.63, 130.02, 128.76, 127.94, 126.58, 125.00, 124.83, 118.57, 118.51, 115.76, 114.62. ESI m/z calculated $[M + H]^+$ for $C_{18}H_{12}BrClN_3OS$ = 431.96, found 432.0 and $[M + H + 2]^+$= 434.0.

3-bromo-2-phenylimidazo[1,2-a]pyridine (37).[51] 2-phenylimidazo[1,2-a]pyridine[49,50] (0.822 g, 4.2 mmol) was dissolved in MeCN (25 mL), and NBS (0.839 g, 4.7 mmol) was added at once. The reaction mixture was stirred at room temperature in the dark until completion by TLC (1.5 h). The reaction mixture was reduced *in vacuo,* and the residue was taken up in DCM (150 mL). The organic layer was washed with 2 M NaOH (80 mL), with a sat. $Na_2S_2O_3$ (100 mL) and H_2O (80 mL). The organic layer was dried over $MgSO_4$ and reduced *in vacuo* to yield the product as a dark oil, which solidified over time to glossy dark crystals (1.13 g, 98% yield). This product was used in the subsequent reactions without further purification. R_f = 0.5 (Heptane/EtOAc) (1: 1) + 1% Et_3N. ^{1}H NMR

https://doi.org/10.1021/acs.jmedchem.0c02163
J. Med. Chem. 2021, 64, 4730−4743

(400 MHz, Chloroform-*d*) δ 8.19 (dt, J = 7.0, 1.1 Hz, 1H), 8.17−8.11 (m, 2H), 7.65 (dt, J = 9.0, 1.1 Hz, 1H), 7.52−7.46 (m, 2H), 7.42−7.36 (m, 1H), 7.29−7.22 (m, 1H), 6.94 (td, J = 6.8, 1.1 Hz, 1H). ^{13}C NMR (151 MHz, Chloroform-*d*) δ 145.61, 142.85, 133.02, 128.61, 128.44, 128.04, 125.22, 124.11, 117.79, 113.19, 91.85. The spectral data were consistent with previously reported data.[52,53] ESI-MS (m/z) calculated $[M + H]^+$ for $C_{13}H_9BrN_2$ = 273.00, found 273.0 and $[M + H + 2]^+$ = 275.0.

3-iodo-2-phenylimidazo[1,2-a]pyridine (38).[54] Obtained via a procedure similar to the synthesis of **37**, from 2-phenylimidazo[1,2-a]pyridine (0.860 g, 4.4 mmol) and *N*-iodosuccinimide (1.15 g, 5.4 mmol.). Also, this reaction was conducted under argon. The product was isolated as a pale brown solid, 1.22 g, 3.8 mmol, 85% yield. This product was used in the subsequent reactions without further purification. R_f = 0.4 (Heptane/EtOAc) (1: 1) + 1% Et_3N. ^{1}H NMR (400 MHz, Chloroform-*d*) δ 8.24 (dt, J = 6.9, 1.2 Hz, 1H), 8.09−8.03 (m, 2H), 7.63 (dt, J = 9.0, 1.1 Hz, 1H), 7.53−7.44 (m, 2H), 7.43−7.37 (m, 1H), 7.27 (ddd, J = 9.0, 6.8, 1.3 Hz, 1H), 6.94 (td, J = 6.8, 1.2 Hz, 1H). ^{13}C NMR (151 MHz, Chloroform-*d*) δ 148.29, 148.25, 133.73, 128.66, 128.49, 128.47, 126.66, 125.66, 117.76, 113.29, 59.57. The spectral data were consistent with previously reported data.[55,56] ESI-MS (m/z) calculated $[M + H]^+$ for $C_{13}H_{10}IN_2$ = 320.99, found 320.9.

2-phenyl-3-((trimethylsilyl)ethynyl)imidazo[1,2-a]pyridine (39). This compound was synthesized from **37** (0.400 g, 1.5 mmol), which was placed in a microwave tube. CuI, (0.043 g, 0.23 mmol, 15 mol %) and $Pd(PPh_3)_2Cl_2$ (0.154 g, 0.22 mmol, 15 mol %) were added. The tube was sealed and purged with argon. Ethynyltrimethylsilane (0.25 mL, 1.8 mmol) and triethylamine (4.5 mL) were added. The reaction mixture was heated to 80 °C until completion by TLC (23 h) and cooled to room temperature. The reaction mixture was diluted with water (30 mL) and Et_2O (100 mL). The aqueous layer was extracted with Et_2O (2 × 80 mL). The combined organic layers were dried over Na_2SO_4 and reduced *in vacuo*. The crude product was concentrated on celite and purified by column chromatography (silica gel 60, 40−63 μM) (PET/EtOAc) (3: 1). The product was isolated as a pale yellow solid (0.211 g, 50% yield). R_f = 0.3 (PET: EtOAc) (3: 1). ^{1}H NMR (400 MHz, Chloroform-*d*) δ 8.39−8.32 (m, 2H), 8.29 (dt, J = 6.8, 1.2 Hz, 1H), 7.65 (dt, J = 8.9, 1.1 Hz, 1H), 7.50−7.42 (m, 2H), 7.41−7.34 (m, 1H), 7.32−7.27 (m, 1H), 6.93 (td, J = 6.8, 1.1 Hz, 1H), 0.35 (s, 9H). ^{13}C NMR (151 MHz, Chloroform-*d*) δ 148.65, 145.16, 133.53, 128.71, 128.56, 127.37, 126.46, 125.47, 117.60, 113.07, 108.17, 105.04, 93.83, 0.07.

2-phenyl-3-(1-phenyl-1H-1,2,3-triazol-4-yl)imidazo[1,2-a]-pyridine (40). A flask was charged with previously lyophilized **39** (0.200 g, 0.69 mmol) and TBAF (0.345 g, 1.3 mmol). The flask was fitted with a rubber septum and purged with argon. Then, dry THF (10 mL) was added through the septum. The reaction mixture was stirred at room temperature until completion by TLC (1.5 h). The reaction mixture was reduced *in vacuo*, and the residue was taken up in a 10% aqueous solution of NH_4Cl (20 mL) and DCM (20 mL). The aqueous layer was extracted with DCM (2 × 20 mL), and the combined organic layers were dried over Na_2SO_4 and reduced *in vacuo* to yield the crude product. The crude product was concentrated on celite and purified by column chromatography (silica gel 60, 40−63 μM) (PET/EtOAc) (2: 1) to furnish 3-ethynyl-2-phenylimidazo-[1,2-a]pyridine as a white solid (0.123 g, 82% yield): mp 141−142 °C (decomp). R_f = 0.4 (PET: EtOAc) (2: 1). ^{1}H NMR (400 MHz, Chloroform-*d*) δ 8.36−8.28 (m, 3H), 7.67 (dt, J = 9.1, 1.1 Hz, 1H), 7.51−7.45 (m, 2H), 7.42−7.36 (m, 1H), 7.30 (ddd, J = 9.1, 6.8, 1.3 Hz, 1H), 6.94 (td, J = 6.8, 1.2 Hz, 1H), 4.07 (s, 1H). ^{13}C NMR (151 MHz, Chloroform-*d*) δ 149.11, 145.41, 133.41, 128.92, 128.76, 127.46, 126.64, 125.39, 117.74, 113.27, 103.96, 90.04, 73.45. A flask was charged with 3-ethynyl-2-phenylimidazo[1,2-a]pyridine (0.114 g, 0.52 mmol), $CuSO_4 \cdot 5H_2O$ (0.0261 g, 0.10 mmol, 20 mol %) and (+)-Sodium L-ascorbate (0.0534 g, 0.27 mmol, 51 mol %). The flask was fitted with a rubber septum and purged with argon. THF (15 mL), H_2O (10 mL), and 1.0 mL of a ∼0.5 M solution of azidobenzene in *tert*-butyl methyl ether (∼0.52 mmol) were then added through the septum. The reaction mixture was stirred at room temperature, in the dark, and monitored by TLC (17.5 h). The reaction mixture was poured into H_2O (100 mL) and EtOAc (100 mL). The aqueous layer was extracted with EtOAc (2 × 100 mL). The combined organic layers were dried over Na_2SO_4 and then reduced *in vacuo*. The crude product was concentrated on celite and purified by column chromatography (40−63 μm silica gel 60) (PET/EtOAc) (1: 1) to yield the product as a white solid (0.137 g, 78% yield): mp 188−189 °C. R_f = 0.6 (PET/EtOAc) (1: 2). R_t = 10.62 min (>99% pure by HPLC system 2). ^{1}H NMR (400 MHz, DMSO-d_6) δ 9.19 (s, 1H), 8.46 (dd, J = 6.9, 1.2 Hz, 1H), 8.05−7.97 (m, 2H), 7.85−7.78 (m, 2H), 7.75−7.71 (m, 1H), 7.65 (dd, J = 8.6, 7.1 Hz, 2H), 7.59−7.51 (m, 1H), 7.45−7.37 (m, 3H), 7.36−7.29 (m, 1H), 7.00 (td, J = 6.8, 1.2 Hz, 1H). ^{13}C NMR (151 MHz, DMSO-d_6) δ 144.79, 143.86, 136.85, 136.48, 133.88, 129.93, 128.96, 128.43, 127.95, 127.76, 125.97, 125.21, 123.81, 120.23, 116.87, 112.97, 110.71. ESI-MS (m/z) calculated $[M + H]^+$ for $C_{21}H_{16}N_5$ = 338.1, found 338.1.

3-(4-chlorophenyl)-5-(2-phenylimidazo[1,2-a]pyridin-3-yl)-1,2,4-oxadiazole (42) 41.[39] (0.171 g, 0.64 mmol) and 4-chloro-N′-hydroxybenzimidamide[40] (0.073 g, 0.43 mmol) were dissolved in DMSO (0.5 mL). Powdered NaOH (0.026 g, 0.63 mmol) was added at once, and the reaction mixture was stirred at room temperature for 7 h and monitored by TLC. Water (8 mL) was added, and the reaction mixture was stirred for 15 min after which the precipitate was collected by filtration and washed with water (15 mL). The solid was dried *in vacuo* and purified by recrystallization from EtOAc (7 mL) and dried *in vacuo* and freeze-dried. The product was isolated as a white solid (0.103 g, 64% yield): mp 242 °C. R_f = 0.8 (DCM/MeOH) (10: 1). R_t = 14.55 min (>98% pure by HPLC 2). This sample was dissolved in 1.0 mL of DMSO. ^{1}H NMR (400 MHz, Chloroform-*d*) δ 9.70 (d, J = 6.9 Hz, 1H), 8.13 (d, J = 8.4 Hz, 2H), 7.93−7.89 (m, 2H), 7.86 (d, J = 9.0 Hz, 1H), 7.59−7.44 (m, 6H), 7.20 (t, J = 6.9 Hz, 1H). ^{13}C NMR (151 MHz, Chloroform-*d*) δ 168.53, 167.21, 152.70, 147.60, 137.69, 132.80, 129.93, 129.78, 129.41, 129.01, 128.76, 128.49, 128.31, 125.32, 117.85, 114.91, 107.54. ESI-MS (m/z) calculated $[M + H]$ for $C_{21}H_{14}ClN_4O$ = 373.09, found 373.1 and $[M + 2 + H]^+$ = 375.1.

Computational Chemistry. *Homology Model.* The model was built using the Maestro Schrödinger, package version 10.7.015, release 2016−3, using *Prime, Structure Prediction Wizard*. The 3.86 Å cryoEM structure of the human $GABA_AR$ $\alpha1\beta2\gamma2$ heteropentamer in complex with GABA and flumazenil (PDB-code: 6D6T) was used as a template for this ECD homology model. In particular, we used the $\alpha1\gamma2$ subunit interface, which contains the bound flumazenil, to avoid modeling a binding site that could not encompass a ligand in the following docking. The human sequences of the ECDs of the $\alpha4$- and δ-subunits (Entries and P48169 and O14764) were extracted from the UniProt database[57] and aligned with the template (Chain D $\alpha1$-subunit and Chain E $\gamma2$-subunit, respectively), using *ClustalW* within Maestro (Figure S4).

The residues 36−43 of the $\alpha4$-subunit and the residues 17−39 of the δ-subunit were deleted as they were poorly modeled because of the lack of a template and expected to be far from the C-loop binding pocket, based on the built monomers. The sequence identities of the ECD of the $\alpha4$- and δ-subunits to the templates were found to be 69 and 36%, respectively.

The model was initially built as monomers using the energy-based method. The monomers were then combined into a heterodimer, using the *Prime Multimer function*. After ensuring correct dimer construction by comparing to the template (Figure S5), the heterodimer was prepared using the *Protein Preparation Wizard*, to fix any problems such as steric clashes.

The expected protonation state of the amino acid residues at pH = 7.4 was then calculated using *PropKa*. Afterward, the model was energy-minimized using *OPLS3* force fields.

The model was assessed by *ProCheck*[58] in which it was found that 88.9, 10.6, and 0.5% of the modeled amino acid residues were in most favored regions, additional allowed regions, and generously allowed regions, respectively (Supporting information). The outliers in the Ramachandran plot and the residues GLU72(A) and GLN162(B)

https://doi.org/10.1021/acs.jmedchem.0c02163
J. Med. Chem. 2021, 64, 4730−4743

were visually inspected and found to be nowhere near the binding site of investigation.

Docking. The ligands were manually drawn within Maestro (Release 2016−3: Maestro, Schrödinger, LLC, New York, NY, 2016) and preprocessed using *LigPrep* (Release 2016−3: LigPrep, Schrödinger, LLC, New York, NY, 2016), and the structures were energy-minimized using *OPLS3* forced fields. The protonation state of the ligands was determined by *Epik* at pH =7.4 ± 2.

To ensure a binding model that can encompass analogues of different sizes from the previous publication,[17] the relatively large 4-butoxy-*N*-(6-chloro-2-(thiophen-2-yl)imidazo[1,2-*a*]pyridin-3-yl)-benzamide was initially docked using induced fit docking (Release 2016−3: Induced Fit Docking protocol; Glide & Prime, Schrödinger, LLC, New York, NY, 2016). The calculations were performed with the *OPLS3* force fields and XP Glide for redocking, and the centroid of the box was specified from the residues, α4R135 and δF90; otherwise, default settings were applied. Among the very similar three top-ranked poses according to the IFD score, we selected the pose with the best Emodel score. The ligand was deleted, and the resulting protein was used as a docking template for XP docking (Release 2016−3: Glide, Schrödinger, LLC, New York, NY, 2016) of a selection of analogues, that is, (*N*-(6-bromo-2-(thiophen-2-yl)-imidazo[1,2-*a*]pyridin-3-yl)-4-methoxybenzamide, *N*-(6,8-dibromo-2-(thiophen-2-yl)imidazo[1,2-*a*]pyridin-3-yl)-4-methoxybenzamide, 4-butoxy-*N*-(6-chloro-2-(thiophen-2-yl)imidazo[1,2-*a*]pyridin-3-yl)-benzamide, and DS2 (Figures S5, S6). The DS2 pose with the best Emodel displayed a binding mode consistent with high scoring poses of the other compounds and was selected for the design of new compounds.

Pharmacology. *Compounds.* GABA and DS2 (4-chloro-N-[2-(2-thienyl)imidazo[1,2-a]pyridin-3-yl]benzamide) were obtained from Tocris Bioscience (Bristol, UK).

Cell Culturing and Transient Transfection. All used HEK293 cell lines were maintained in DMEM containing Gluta-MAX-I supplemented with 10% fetal bovine serum and 1% penicillin−streptomycin (all from Life Technologies, Paisley, UK) in an incubator at 37 °C with a humidity of 5% CO_2. The HEK293 Flp-In cell line stably expressing the human δ-subunit (δ-HEK) and the background HEK cell line stably expressing the G-protein coupled receptor NPBWR2 were positively selected using 200 μg/mL hygromycin B as reported previously.[59]

The $\alpha4\beta1\delta$ receptor was selected as the model receptor based on previous success with establishing a reproducible, uniform receptor population for this subtype.[59] Recombinant human $\alpha4\beta1\delta$ and $\alpha4\beta1\gamma2$ $GABA_A$Rs were expressed by transfection of δ-HEK cells and HEK background cells, respectively. δ-HEK cells were transfected in a 1:1 ratio of human α_4- and β_1-subunits (pUNIV) to express $\alpha4\beta1\delta$ as described previously.[59] HEK background cells were transfected in a 1:1:2 ratio of human α4-, β1-, and γ2-subunit (pcDNA3.1/Zeo) to express $\alpha4\beta1\gamma2$ using Polyfect transfection reagent (Qiagen, West Sussex, UK) as described by the manufacturer, except for using half volumes. A cell line stably expressing $\alpha1\beta2\gamma2$ receptors in HEK293 cells as previously used[59] was a gift from Marianne L. Jensen, Neurosearch.

FMP Assay. Testing of compounds in the fluorescence-based FMP assay was performed exactly as described previously.[59] Data were obtained as relative changes in fluorescence units (ΔRFU) given as the difference between the baseline fluorescence signal before compound addition and the peak/top plateau in the fluorescence signal obtained after buffer/compound addition. All raw data traces were inspected manually, and signals resulting from buffer/compound additions and signal artifacts were omitted from the analysis. Generally, we could confirm the presence of the γ2 subunit in the functional receptors from the higher response level and numerically lower GABA potencies at $\alpha4\beta1\gamma2$ compared to $\alpha4\beta1$ binary receptors in the FMP assay.

For agonist testing, the obtained ΔRFU responses were normalized to the ΔRFU response induced by 100 μM GABA (maximum response) after subtraction of the buffer response and given as % Response of $GABA_{max}$. When testing for the PAM effect, the analogues were coapplied with a concentration of GABA corresponding to approximately GABA EC_{20} values determined from full GABA concentration−response curves at the respective receptor subtypes (see Table 1). The obtained ΔRFU responses were normalized to the ΔRFU response induced by 100 μM GABA (maximum response) after subtraction of the buffer response and given as %Response of $GABA_{max}$.

Concentration−response curves used to determine the PAM potencies (EC_{50}-values) of the analogues and the agonist potencies of GABA used to determine GABA EC_{20} values were fitted to the four-parameter concentration−response model:

$$\text{Response} = \text{bottom} + \frac{\text{top} - \text{bottom}}{1 + 10^{[(\log EC_{50} - A)\cdot n_H]}}$$

where EC_{50} is the concentration of the compound A resulting in the half-maximum response (response halfway between top and bottom) and n_H is the Hill coefficient of the curve. The data analysis was performed using GraphPad Prism v. 8.4.3 (GraphPad software Inc., San Diego, CA, USA).

■ ASSOCIATED CONTENT

Supporting Information

The Supporting Information is available free of charge at https://pubs.acs.org/doi/10.1021/acs.jmedchem.0c02163.

Structural comparison of the employed homology model template and published templates (S1), structural comparison of the binding modes of DS2 (S2), representative concentration−response curves of the PAM activity of **30**−**32**, **35**, and **36** (S3), the sequence alignment (S4), structural comparison of the homology model (S5), and structural illustration of the binding of **30**−**32** (S6) (PDF)

Molecular formula string (CSV)

■ AUTHOR INFORMATION

Corresponding Author

Bente Frølund − *Department of Drug Design and Pharmacology, Faculty of Health and Medical Sciences, University of Copenhagen, Copenhagen DK-2100, Denmark;* orcid.org/0000-0001-5476-6288; Phone: +45.35336495; Email: bfr@sund.ku.dk

Authors

Frederik Rostrup − *Department of Drug Design and Pharmacology, Faculty of Health and Medical Sciences, University of Copenhagen, Copenhagen DK-2100, Denmark*

Christina B. Falk-Petersen − *Department of Drug Design and Pharmacology, Faculty of Health and Medical Sciences, University of Copenhagen, Copenhagen DK-2100, Denmark*

Kasper Harpsøe − *Department of Drug Design and Pharmacology, Faculty of Health and Medical Sciences, University of Copenhagen, Copenhagen DK-2100, Denmark*

Stine Buchleithner − *Department of Drug Design and Pharmacology, Faculty of Health and Medical Sciences, University of Copenhagen, Copenhagen DK-2100, Denmark*

Irene Conforti − *Department of Drug Design and Pharmacology, Faculty of Health and Medical Sciences, University of Copenhagen, Copenhagen DK-2100, Denmark*

Sascha Jung − *Institute of Pharmaceutical and Biomedical Sciences, Johannes Gutenberg University Mainz, Mainz D-55128, Germany*

David E. Gloriam − *Department of Drug Design and Pharmacology, Faculty of Health and Medical Sciences,*

University of Copenhagen, Copenhagen DK-2100, Denmark; orcid.org/0000-0002-4299-7561

Tanja Schirmeister − *Institute of Pharmaceutical and Biomedical Sciences, Johannes Gutenberg University Mainz, Mainz D-55128, Germany*

Petrine Wellendorph − *Department of Drug Design and Pharmacology, Faculty of Health and Medical Sciences, University of Copenhagen, Copenhagen DK-2100, Denmark;* orcid.org/0000-0002-5455-8013

Complete contact information is available at: https://pubs.acs.org/10.1021/acs.jmedchem.0c02163

Author Contributions

The manuscript was written through contributions of all authors. F.R. and K.H. performed the modeling studies. F.R., I.C., and S.J. synthesized the compounds. C.F.P., S.B., and P.W. performed FMP assays. B.N. performed radioligand binding assay. B.F. devised the study and supervised the work together with P.W. All authors have given approval to the final version of the manuscript.

Notes

The authors declare no competing financial interest.

■ ACKNOWLEDGMENTS

This work was supported by a Lundbeck Foundation (grant R230-2016-2562 to C.B.F.-P.) and the Drug Research Academy.

■ ABBREVIATIONS

CryoEM, Cryogenic Electron Microscopy; ECD, extracellular domain; FMP, fluorometric imaging plate reader (FLIPR) membrane potential; GABA, γ-aminobutyric acid; $GABA_ARs$, γ-aminobutyric acid type A receptors; [^{3}H]-EBOB, [^{3}H]-ethynylbicyclooethobenzoate; PAM, positive allosteric modulator; SEM, Standard Error of the Mean; SAR, structure−activity relationship; XP, Xtra precision.

■ REFERENCES

(1) Owens, D. F.; Kriegstein, A. R. Is there more to gaba than synaptic inhibition? *Nat. Rev. Neurosci.* **2002**, *3*, 715−727.

(2) Tija, C. J.; Guido, M. GABAA receptor trafficking and its role in the dynamic modulation of neuronal inhibition. *Nat. Rev. Neurosci.* **2008**, *9*, 331−343.

(3) Chiara, D. C.; Jounaidi, Y.; Zhou, X.; Savechenkov, P. Y.; Bruzik, K. S.; Miller, K. W.; Cohen, J. B. General anesthetic binding sites in human α4β3δ γ-aminobutyric acid type A receptors (GABAARs). *J. Biol. Chem.* **2016**, *291*, 26529−26539.

(4) Hanson, S. M.; Czajkowski, C. Structural mechanisms underlying benzodiazepine modulation of the GABA(A) receptor. *J. Neurosci.* **2008**, *28*, 3490−3499.

(5) Möhler, H.; Fritschy, J. M.; Rudolph, U. A new benzodiazepine pharmacology. *J. Pharmacol. Exp. Ther.* **2002**, *300*, 2−8.

(6) Gravielle, M. C. Regulation of GABAA receptors by prolonged exposure to endogenous and exogenous ligands. *Neurochem. Int.* **2018**, *118*, 96−104.

(7) Farrant, M.; Nusser, Z. Variations on an inhibitory theme: phasic and tonic activation of GABAA receptors. *Nat. Rev. Neurosci.* **2005**, *6*, 215−229.

(8) Chuang, S.-H.; Reddy, D. S. Genetic and molecular regulation of extrasynaptic GABA-A receptors in the brain: Therapeutic insights for epilepsy. *J. Pharmacol. Exp. Ther.* **2018**, *364*, 180−197.

(9) Roberto, M.; Varodayan, F. P. Synaptic targets: Chronic alcohol actions. *Neuropharmacology* **2017**, *122*, 85−99.

(10) Holm, M. M.; Nieto-Gonzalez, J. L.; Vardya, I.; Henningsen, K.; Jayatissa, M. N.; Wiborg, O.; Jensen, K. Hippocampal GABAergic dysfunction in a rat chronic mild stress model of depression. *Hippocampus* **2011**, *21*, 422−433.

(11) Brickley, S. G.; Mody, I. Extrasynaptic GABA(A) receptors: their function in the CNS and implications for disease. *Neuron* **2012**, *73*, 23−34.

(12) Lee, V.; Maguire, J. The impact of tonic GABAA receptor-mediated inhibition on neuronal excitability varies across brain region and cell type. *Front. Neural Circuits* **2014**, *8*, 1−27.

(13) Solomon, V. R.; Tallapragada, V. J.; Chebib, M.; Johnston, G. A. R.; Hanrahan, J. R. GABA allosteric modulators: An overview of recent developments in non-benzodiazepine modulators. *Eur. J. Med. Chem.* **2019**, *171*, 434−461.

(14) Lee, H. J.; Absalom, N. L.; Hanrahan, J. R.; van Nieuwenhuijzen, P.; Ahring, P. K.; Chebib, M. A pharmacological characterization of GABA, THIP and DS2 at binary alpha4beta3 and beta3delta receptors: GABA activates beta3delta receptors via the beta3(+)delta(−) interface. *Brain Res.* **2016**, *1644*, 222−230.

(15) Jensen, M. L.; Wafford, K. A.; Brown, A. R.; Belelli, D.; Lambert, J. J.; Mirza, N. R. A study of subunit selectivity, mechanism and site of action of the delta selective compound 2 (DS2) at human recombinant and rodent native GABAA receptors. *Br. J. Pharmacol.* **2013**, *168*, 1118−1132.

(16) L'Estrade, E. T.; Hansen, H. D.; Falk-Petersen, C.; Haugaard, A.; Griem-Krey, N.; Jung, S.; Lüddens, H.; Schirmeister, T.; Erlandsson, M.; Ohlsson, T.; Knudsen, G. M.; Herth, M. M.; Wellendorph, P.; Frølund, B. Synthesis and pharmacological evaluation of [11C]4-Methoxy-N-[2-(thiophen-2-yl)imidazo[1,2-a]-pyridin-3-yl]benzamide as a brain penetrant PET ligand selective for the δ-subunit-containing γ-aminobutyric acid type A receptors. *ACS Omega* **2019**, *4*, 8846−8851.

(17) Yakoub, K.; Jung, S.; Sattler, C.; Damerow, H.; Weber, J.; Kretzschmann, A.; Cankaya, A. S.; Piel, M.; Rösch, F.; Haugaard, A. S.; Frølund, B.; Schirmeister, T.; Lüddens, H. Structure−function evaluation of imidazopyridine derivatives selective for δ-subunit-containing γ-aminobutyric acid type A (GABAA) receptors. *J. Med. Chem.* **2018**, *61*, 1951−1968.

(18) Cole, L. M.; Casida, J. E. GABA-gated chloride channel: binding-site for 4′-ethynyl-4-n-[2,3-3H2]propylbicycloorthobenzoate. *Pestic. Biochem. Physiol.* **1992**, *44*, 1−8.

(19) Uusi-Oukari, M.; Maksay, G. Allosteric modulation of [3H]EBOB binding to GABAA receptors by diflunisal analogues. *Neurochem. Int.* **2006**, *49*, 676−682.

(20) Yagle, M. A.; Martin, M. W.; de Fiebre, C. M.; de Fiebre, N. C.; Drewe, J. A.; Dillon, G. H. [3H]Ethynylbicycloorthobenzoate ([3H]EBOB) binding in recombinant GABAA receptors. *Neurotoxicology* **2003**, *24*, 817−824.

(21) Maksay, G.; Biro, T. High affinity, heterogeneous displacement of [3H]EBOB binding to cerebellar GABA A receptors by neurosteroids and GABA agonists. *Neuropharmacology* **2005**, *49*, 431−438.

(22) Stephen, G. B.; Zhiwen, E.; Thomas, P. M.; Catriona, M. H. The contribution of delta subunit-containing GABAA receptors to phasic and tonic conductance changes in cerebellum, thalamus and neocortex. *Front. Neural Circuits* **2013**, *7*, 1−8.

(23) Hartiadi, L. Y.; Ahring, P. K.; Chebib, M.; Absalom, N. L. High and low GABA sensitivity α4β2δ GABAA receptors are expressed in Xenopus laevis oocytes with divergent stoichiometries. *Biochem. Pharmacol.* **2016**, *103*, 98−108.

(24) Masiulis, S.; Desai, R.; Uchański, T.; Serna Martin, I.; Laverty, D.; Karia, D.; Malinauskas, T.; Zivanov, J.; Pardon, E.; Kotecha, A.; Steyaert, J.; Miller, K. W.; Aricescu, A. R. GABAA receptor signalling mechanisms revealed by structural pharmacology. *Nature* **2019**, *565*, 454−459.

(25) Ahring, P. K.; Bang, L. H.; Jensen, M. L.; Strøbæk, D.; Hartiadi, L. Y.; Chebib, M.; Absalom, N. A pharmacological assessment of agonists and modulators at α4β2γ2 and α4β2δ GABAA receptors:

The challenge in comparing apples with oranges. *Pharmacol. Res.* **2016**, *111*, 563−576.
(26) Kaur, K. H.; Baur, R.; Sigel, E. Unanticipated structural and functional properties of delta-subunit-containing GABAA receptors. *J. Biol. Chem.* **2009**, *284*, 7889−7896.
(27) Baur, R.; Kaur, K. H.; Sigel, E. Structure of alpha6 beta3 delta GABAA receptors and their lack of ethanol sensitivity. *J. Neurochem.* **2009**, *111*, 1172−1181.
(28) Barrera, N. P.; Betts, J.; You, H.; Henderson, R. M.; Martin, I. L.; Dunn, S. M. J.; Edwardson, J. M. Atomic force microscopy reveals the stoichiometry and subunit arrangement of the alpha4beta3delta GABA(A) receptor. *Mol. Pharmacol.* **2008**, *73*, 960−967.
(29) Patel, B.; Mortensen, M.; Smart, T. G. Stoichiometry of δ subunit containing GABAA receptors. *Br. J. Pharmacol.* **2014**, *171*, 985−994.
(30) Zhu, S.; Noviello, C. M.; Teng, J.; Walsh, R. M., Jr.; Kim, J. J.; Hibbs, R. E. Structure of a human synaptic GABAA receptor. *Nature* **2018**, *559*, 67−72.
(31) Bienaymé, H.; Bouzid, K. A new heterocyclic multicomponent reaction for the combinatorial synthesis of fused 3-aminoimidazoles. *Angew. Chem., Int. Ed.* **1998**, *37*, 2234−2237.
(32) Groebke, K.; Weber, L.; Mehlin, F. Synthesis of imidazo[1,2-a] annulated pyridines, pyrazines and pyrimidines by a novel three-component condensation. *Synlett* **1998**, *1998*, 661−663.
(33) Blackburn, C.; Guan, B.; Fleming, P.; Shiosaki, K.; Tsai, S. Parallel synthesis of 3-aminoimidazo[1,2-a]pyridines and pyrazines by a new three-component condensation. *Tetrahedron Lett.* **1998**, *39*, 3635−3638.
(34) Guchhait, S. K.; Chaudhary, V.; Madaan, C. A chemoselective Ugi-type reaction in water using TMSCN as a functional isonitrile equivalent: generation of heteroaromatic molecular diversity. *Org. Biomol. Chem.* **2012**, *10*, 9271−9277.
(35) Bazin, M.-A.; Marhadour, S.; Tonnerre, A.; Marchand, P. Exploration of versatile reactions on 2-chloro-3-nitroimidazo[1,2-a]pyridine: expanding structural diversity of C2- and C3-functionalized imidazo[1,2-a]pyridines. *Tetrahedron Lett.* **2013**, *54*, 5378−5382.
(36) Misra, A. P.; Raj, K.; Bhaduri, A. P. In search of imidazo [1,2-a] pyridine derivatives exhibiting resistance for catalytic hydrogenation. *Synth. Commun.* **1999**, *29*, 3227−3236.
(37) Tokuhara, H.; Imaeda, Y.; Fukase, Y.; Iwanaga, K.; Taya, N.; Watanabe, K.; Kanagawa, R.; Matsuda, K.; Kajimoto, Y.; Kusumoto, K.; Kondo, M.; Snell, G.; Behnke, C. A.; Kuroita, T. Discovery of benzimidazole derivatives as orally active renin inhibitors: Optimization of 3,5-disubstituted piperidine to improve pharmacokinetic profile. *Bioorg. Med. Chem.* **2018**, *26*, 3261−3286.
(38) El Akkaoui, A.; Bassoude, I.; Koubachi, J.; Berteina-Raboin, S.; Mouaddib, A.; Guillaumet, G. Pd-catalyzed regiocontrolled Sonogashira and Suzuki cross-coupling reaction of 3,6-dihalogenoimidazo-[1,2-a]pyridines: one-pot double-coupling approach. *Tetrahedron* **2011**, *67*, 7128−7138.
(39) Huo, C.; Tang, J.; Xie, H.; Wang, Y.; Dong, J. CBr4 Mediated Oxidative C−N Bond Formation: Applied in the synthesis of imidazo[1,2-α]pyridines and imidazo[1,2-α]pyrimidines. *Org. Lett.* **2016**, *18*, 1016−1019.
(40) Mayer, J.; Sauer, A.; Iglesias, B. A.; Acunha, T. V.; Back, D.; Rodrigues, O.; Dornelles, L. Ferrocenylethenyl-substituted 1,3,4-oxadiazolyl-1,2,4-oxadiazoles: Synthesis, characterization and DNA-binding assays. *J. Organometal. Chem.* **2017**, *841*, 1−11.
(41) Schwartz, T. W.; Holst, B. Allosteric enhancers, allosteric agonists and ago-allosteric modulators: where do they bind and how do they act? *Trends Pharmacol. Sci.* **2007**, *28*, 366−373.
(42) Madjroh, N.; Olander, E. R.; Bundgaard, C.; Soderhielm, P. C.; Jensen, A. A. Functional properties and mechanism of action of PPTQ, an allosteric agonist and low nanomolar positive allosteric modulator at GABAA receptors. *Biochem. Pharmacol.* **2018**, *147*, 153−169.
(43) Gill, J. K.; Dhankher, P.; Sheppard, T. D.; Sher, E.; Millar, N. S. A series of alpha7 nicotinic acetylcholine receptor allosteric modulators with close chemical similarity but diverse pharmacological properties. *Mol. Pharmacol.* **2012**, *81*, 710−718.
(44) Dalby, N. O.; Falk-Petersen, C. B.; Leurs, U.; Scholze, P.; Krall, J.; Frolund, B.; Wellendorph, P. Silencing of spontaneous activity at alpha4beta1/3delta GABAA receptors in hippocampal granule cells reveals different ligand pharmacology. *Br. J. Pharmacol.* **2020**, *177*, 3975−3990.
(45) Martínez-Urbina, M. A.; Zentella, A.; Vilchis-Reyes, M. A.; Guzmán, Á.; Vargas, O.; Ramírez Apan, M. T.; Ventura Gallegos, J. L.; Díaz, E. 6-Substituted 2-(N-trifluoroacetylamino)imidazopyridines induce cell cycle arrest and apoptosis in SK-LU-1 human cancer cell line. *Eur. J. Med. Chem.* **2010**, *45*, 1211−1219.
(46) Schwerkoske, J.; Masquelin, T.; Perun, T.; Hulme, C. New multi-component reaction accessing 3-aminoimidazo[1,2-a]pyridines. *Tetrahedron Lett.* **2005**, *46*, 8355−8357.
(47) Yan, R.-L.; Yan, H.; Ma, C.; Ren, Z.-Y.; Gao, X.-A.; Huang, G.-S.; Liang, Y.-M. Cu(I)-Catalyzed synthesis of imidazo[1,2-a]pyridines from aminopyridines and nitroolefins using air as the oxidant. *J. Org. Chem.* **2012**, *77*, 2024−2028.
(48) Reynoso Lara, J. E.; Salgado-Zamora, H.; Bazin, M.-A.; Campos-Aldrete, M. E.; Marchand, P. Design and synthesis of imidazo[1,2-a]pyridines with carboxamide group substitution and in silico evaluation of their interaction with a LuxR-type quorum sensing receptor. *J. Heterocyclic Chem.* **2018**, *55*, 1101−1111.
(49) Kour, D.; Khajuria, R.; Kapoor, K. K. Iodine-ammonium acetate promoted reaction between 2-aminopyridine and aryl methyl ketones: a novel approach towards the synthesis of 2-arylimidazo[1,2-a]pyridines. *Tetrahedron Lett.* **2016**, *57*, 4464−4467.
(50) Sayeed, I. B.; Lakshma Nayak, V.; Shareef, M. A.; Chouhan, N. K.; Kamal, A. Design, synthesis and biological evaluation of imidazopyridine−propenone conjugates as potent tubulin inhibitors. *Med. Chem. Commun.* **2017**, *8*, 1000−1006.
(51) Salgado-Zamora, H.; Velazquez, M.; Mejía, D.; Campos-Aldrete, M. E.; Jimenez, R.; Cervantes, H. Influence of the 2-aryl group on the ipso electrophilic substitution process of 2-arylimidazo-[1,2-a]pyridines. *Heterocycl. Commun.* **2008**, *14*, 27−32.
(52) Zhou, X.; Yan, H.; Ma, C.; He, Y.; Li, Y.; Cao, J.; Yan, R.; Huang, G. Copper-mediated aerobic oxidative synthesis of 3-bromoimidazo[1,2-a]pyridines with pyridines and enamides. *J. Org. Chem.* **2016**, *81*, 25−31.
(53) Delaye, P. O.; Pénichon, M.; Allouchi, H.; Enguehard-Gueiffier, C.; Gueiffier, A. Regiocontrolled functionalization of 2,3-dihalogenoimidazo[1,2- a]pyridines by SuzukiMiyaura and Sonogashira cross-coupling reactions. *Org. Biomol. Chem.* **2017**, *15*, 4199−4204.
(54) Ghosh, P.; Ganguly, B.; Kar, B.; Dwivedi, S.; Das, S. Green procedure for highly efficient, rapid synthesis of imidazo[1,2-a]pyridine and its late stage functionalization. *Synth. Commun.* **2018**, *48*, 1076−1084.
(55) Zhang, Y.; Chen, Z.; Wu, W.; Zhang, Y.; Su, W. CuI-catalyzed aerobic oxidative α-aminaton cyclization of ketones to access aryl or alkenyl-substituted imidazoheterocycles. *J. Org. Chem.* **2013**, *78*, 12494−12504.
(56) Chen, Z.; Cao, G.; Zhang, F.; Li, H.; Xu, J.; Miao, M.; Ren, H. Metal-free mediated C-3 methylsulfanylation of imidazo[1,2-a]-pyridines with dimethyl sulfoxide as a methylsulfanylating agent. *Synlett* **2017**, *28*, 1795−1800.
(57) The UniProt Consortium. UniProt: a worldwide hub of protein knowledge. *Nucleic Acids Res.* **2019**, *47*, D506−D515.
(58) Laskowski, R. A.; MacArthur, M. W.; Moss, D. S.; Thornton, J. M. PROCHECK: a program to check the stereochemical quality of protein structures. *J. Appl. Crystallogr.* **1993**, *26*, 283−291.
(59) Falk-Petersen, C. B.; Søgaard, R.; Madsen, K. L.; Klein, A. B.; Frølund, B.; Wellendorph, P. Development of a robust mammalian cell-based assay for studying recombinant α β δ GABA receptor subtypes. *Basic Clin. Pharmacol. Toxicol.* **2017**, *121*, 119−129.

https://doi.org/10.1021/acs.jmedchem.0c02163
J. Med. Chem. 2021, 64, 4730−4743